



THE UNIVERSITY *of* EDINBURGH

Edinburgh Research Explorer

Epicardial cell shape and maturation are regulated by Wt1 via transcriptional control of Bmp4

Citation for published version:

Velecela, V, Torres-Cano, A, García-Melero, A, Ramiro-Pareta, M, Müller-Sánchez, C, Segarra-Mondejar, M, Chau, Y-Y, Campos-Bonilla, B, Reina, M, Soriano, FX, Hastie, N, Martínez, FO & Martínez-Estrada, OM 2019, 'Epicardial cell shape and maturation are regulated by Wt1 via transcriptional control of Bmp4', *Development*, vol. 146, no. 20. <https://doi.org/10.1242/dev.178723>

Digital Object Identifier (DOI):

[10.1242/dev.178723](https://doi.org/10.1242/dev.178723)

Link:

[Link to publication record in Edinburgh Research Explorer](#)

Document Version:

Publisher's PDF, also known as Version of record

Published In:

Development

General rights

Copyright for the publications made accessible via the Edinburgh Research Explorer is retained by the author(s) and / or other copyright owners and it is a condition of accessing these publications that users recognise and abide by the legal requirements associated with these rights.

Take down policy

The University of Edinburgh has made every reasonable effort to ensure that Edinburgh Research Explorer content complies with UK legislation. If you believe that the public display of this file breaches copyright please contact openaccess@ed.ac.uk providing details, and we will remove access to the work immediately and investigate your claim.



RESEARCH ARTICLE

Epicardial cell shape and maturation are regulated by *Wt1* via transcriptional control of *Bmp4*

Víctor Velecela^{1,2}, Alejo Torres-Cano^{1,3}, Ana García-Melero^{1,3}, Marina Ramiro-Pareta^{1,3}, Claudia Müller-Sánchez¹, Marc Segarra-Mondejar^{1,4}, You-Ying Chau⁵, Begoña Campos-Bonilla⁶, Manuel Reina¹, Francesc X. Soriano^{1,4}, Nicholas D. Hastie², Fernando O. Martínez⁷ and Ofelia M. Martínez-Estrada^{1,3,*}

ABSTRACT

The epicardium plays a crucial role in embryonic heart development and adult heart repair; however, the molecular events underlying its maturation remain unknown. *Wt1*, one of the main markers of the embryonic epicardium, is essential for epicardial development and function. Here, we analyse the transcriptomic profile of epicardial-enriched cells at different stages of development and from control and epicardial-specific *Wt1* knockout (*Wt1KO*) mice. Transcriptomic and cell morphology analyses of epicardial cells from epicardial-specific *Wt1KO* mice revealed a defect in the maturation process of the mutant epicardium, including sustained upregulation of *Bmp4* expression and the inability of mutant epicardial cells to transition into a mature squamous phenotype. We identified *Bmp4* as a transcriptional target of *Wt1*, thus providing a molecular basis for the retention of the cuboidal cell shape observed in the *Wt1KO* epicardium. Accordingly, inhibition of the *Bmp4* signalling pathway both *ex vivo* and *in vivo* rescued the cuboidal phenotype of the mutant epicardium. Our findings indicate the importance of the cuboidal-to-squamous transition in epicardial maturation, a process regulated by *Wt1*.

KEY WORDS: Epicardium, *Wt1*, BMP4, Heart morphogenesis, Cell shape, Mesothelium, Mouse

INTRODUCTION

Detailed knowledge of the differentiation and maturation steps presented by various cell types in the embryonic heart is key to achieving a proper understanding of both normal and abnormal cardiovascular development.

The epicardium, the coelomic epithelium of the heart, forms from a transitory cluster of cells called the proepicardium (PE), which

migrates to the heart in mice at embryonic day (E)9.5 and completely covers the myocardial surface by E11.5. Once the epicardium is formed, these cells provide paracrine signals that influence both myocardial and coronary blood vessel development (Perez-Pomares and de la Pompa, 2011).

Around E13.5, a subset of epicardial cells undergoes an epicardial epithelium-to-mesenchymal transition (EMT) that induces the formation of epicardial-derived cells (EPDCs), a population of plastic mesenchymal cardiac progenitor cells that differentiate mainly into fibroblasts and coronary vascular smooth muscle cells (Perez-Pomares and de la Pompa, 2011).

Later on in development, by stage E15.5, the heart has almost achieved its definitive prenatal configuration (Miquerol and Kelly, 2013) and the epicardium decreases its proliferation rate until adulthood, when it becomes quiescent (Wu et al., 2010). These changes in epicardial properties correlate with a downregulation of *Raldh2* (*Aldh1a2*) and *Wt1*, genes abundantly expressed in the embryonic epicardium that are almost completely turned off in the adult epicardium (Smart et al., 2011; Zhou et al., 2011).


Interest in the study of the epicardium has grown considerably in recent years, probably largely as a result of the reactivation of the epicardium following heart damage. Interestingly, one of the main hallmarks of this reactivation is the upregulation of genes involved in embryonic epicardial development, such as *Wt1* and *Raldh2*, two genes for which expression correlates with the proliferation and expansion of the epicardium in the damaged area (Lepilina et al., 2006; Porrello et al., 2011; van Wijk et al., 2012; Zhou et al., 2011).

Wilms' tumour suppressor gene 1 (*Wt1*) encodes a zinc-finger protein, which plays a crucial role in the formation of several organs during embryonic development (Hastie, 2017). It is also essential for the integrity and functioning of multiple adult tissues (Chau et al., 2011). In the developing heart, *Wt1* is expressed mainly in the epicardium and EPDCs and is one of the main hallmarks of the embryonic epicardial signature of the reactivated epicardium following myocardial infarction (MI) (van Wijk et al., 2012; Zhou et al., 2011). *Wt1* was previously presumed to be essential for heart development (Moore et al., 1999), but this was confirmed only recently, when *Wt1* was deleted in an epicardial-specific manner (Martínez-Estrada et al., 2010). The loss of *Wt1* in the epicardium impairs the formation of EPDCs, and this is probably one of the main causes for the defective formation of the coronary vasculature observed in this knockout mouse model (Martínez-Estrada et al., 2010).

Here, we carried out a genome-wide transcriptomic analysis of *in vivo* isolated epicardial-enriched cells (*Wt1GFP⁺⁺* epicardial-enriched cell population) at different stages of development. In addition, we also compared the transcriptomic profile of epicardial-enriched cells from control and epicardial-specific *Wt1* knockout mice, referred to hereafter as *epiWt1KO* (Martínez-Estrada et al.,

¹Celltec-UB, Department of Cell Biology, Physiology and Immunology, Faculty of Biology, University of Barcelona, Barcelona 08028, Spain. ²MRC Human Genetics Unit, Institute of Genetics and Molecular Medicine, Edinburgh EH4 2XU, UK. ³Institute of Biomedicine (IBUB), University of Barcelona, Barcelona 08028, Spain. ⁴Institut de Neurociències, Universitat de Barcelona, Barcelona 08028, Spain. ⁵Centre for Cardiovascular Science, The Queen's Medical Research Institute, University of Edinburgh, Edinburgh EH16 4TJ, UK. ⁶Department of Basic Clinical Practice, University of Barcelona, Barcelona 08036, Spain. ⁷School of Biosciences and Medicine, Faculty of Health and Medical Sciences, University of Surrey, Guildford GU2 7XH, UK.

*Author for correspondence (ofeliarmartinez@ub.edu)

 V.V., 0000-0001-5837-4935; A.T.-C., 0000-0003-4857-3177; A.G.-M., 0000-0002-0574-0417; M.R.-P., 0000-0002-9017-4981; C.M.-S., 0000-0003-2748-6357; M.S.-M., 0000-0001-7376-7104; Y.-Y.C., 0000-0002-8561-8365; B.C.-B., 0000-0002-4993-0327; M.R., 0000-0002-0701-200X; F.X.S., 0000-0003-1678-7162; N.D.H., 0000-0002-0515-168X; F.O.M., 0000-0003-0908-9366; O.M.M.-E., 0000-0002-1814-1974

2010). Transcriptomic and cell morphology analyses of the epicardium in *epiWt1KO* revealed a defect in the maturation process of the mutant epicardium that leads to a sustained upregulation of *Bmp4* expression and an inability of mutant epicardial cells to transition into a mature squamous phenotype. We identified *Bmp4* as a transcriptional target of *Wt1*, thus providing a molecular basis for the retention of the cuboidal cell shape observed in the *Wt1KO* epicardium. Accordingly, inhibition of the BMP4 signalling pathway both *ex vivo* and *in vivo* rescued the cuboidal phenotype found in the mutant epicardium. Our data provide important new insights into the successive waves of cellular transitions required for the formation of the epicardium, including maturation, and the role of *Wt1* in this process.

RESULTS

Isolation of a population of epicardial-enriched cells during heart development

Despite growing interest in the study of the epicardium, a detailed profile that interrogates its cellular dynamics through different stages of embryonic development remains missing (Simoes and Riley, 2018). To investigate this, we decided to isolate and characterise the global expression profiles of *Wt1*-positive epicardial cells during embryonic heart development using *Wt1*-GFP knock-in mice (*Wt1^{GFP}*) (Hosen et al., 2007).

Fluorescence-activated cell sorting (FACS) analyses of enzymatically disaggregated E11.5 embryonic hearts from

Wt1^{GFP} mice revealed two distinct types of *Wt1*-GFP-positive cells based on their GFP expression levels (Fig. 1A,B): a *Wt1*-GFP bright population (hereafter called *Wt1GFP⁺⁺*) and a *Wt1*-GFP dim population (hereafter *Wt1GFP⁺*) (Fig. 1B). These mice have previously been characterised; the GFP is expressed under the endogenous transcriptional regulatory elements of the *Wt1* gene (Hosen et al., 2007) and the GFP in the embryonic heart is expressed mainly in the epicardium and EPDCs (Fig. S1A) (Martinez-Estrada et al., 2010). Quantitative RT-PCR (qRT-PCR) analyses for *Wt1* expression in these populations confirmed that GFP expression levels correlate with the endogenous expression of the *Wt1* gene (Fig. 1C).

The presence of two populations of *Wt1*-GFP-positive cells at such an early stage prompted us to study their gene expression programmes. A transcriptomic analysis demonstrated that *Wt1GFP⁺⁺* and *Wt1GFP⁺* cells represent two cell populations with distinct profiles: 594 transcripts (505 unique genes) were more abundant in the *Wt1GFP⁺⁺* population and 652 transcripts (536 unique genes) were more abundant in the *Wt1GFP⁺* population (Table S1) (see Materials and Methods for details of the differential expression analysis). qRT-PCR analysis was used to confirm five genes in each signature: we confirmed that *Wt1GFP⁺⁺* cells express high levels of epicardial genes, such as *Upk3b*, *Upk1b*, *Tcf21*, *Dlk1* and *Dcn*, whereas the *Wt1GFP⁺* population overexpressed cardiac structural genes, such as *Actc1*, *Actn2*, *Myh6*, *Ttn* and the atrial natriuretic peptide gene *Nppa* (Fig. 1D).

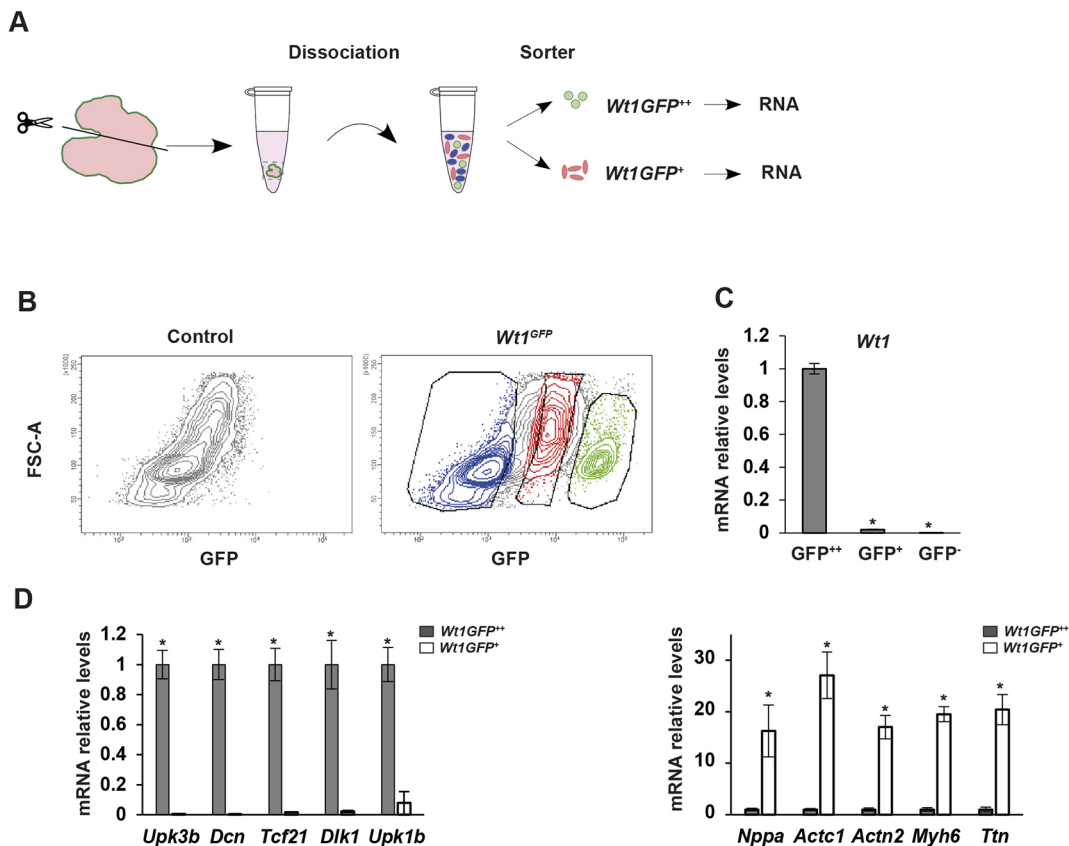


Fig. 1. Isolation of a population of epicardial-enriched cells during heart development. (A) Schematic of the isolation of *Wt1GFP*-positive cells from embryonic hearts from *Wt1^{GFP}* mice. (B) FACS analyses of enzymatically digested E11.5 hearts from *Wt1^{GFP}* mice revealed two distinct types of *Wt1GFP*-positive cells: *Wt1*-GFP⁺⁺ (green) and *Wt1*-GFP⁺ (red), and a negative population (blue). A plot of a negative-control GFP littermate heart is also shown. (C) qRT-PCR analysis of *Wt1* expression in the sorted populations of cells. Values represent mean±s.e.m. **P*<0.05, one-way ANOVA followed by Tukey's post-hoc test. (D) qRT-PCR analysis of the indicated genes in *Wt1GFP⁺⁺* and *Wt1GFP⁺* sorted cells. Values represent mean±s.e.m. **P*<0.05, two-tailed Student's *t*-test. RNA from FACS-sorted isolated cells from at least ten embryonic hearts was pooled to make one replicate, and three replicates per condition were used for the analysis.

Taken together, these data demonstrate that *Wt1GFP⁺⁺* cells represent a population of cells highly enriched in epicardial cells, but further research is needed for a complete overview of the source and nature of the *Wt1GFP⁺* population of cells.

Molecular signature of *Wt1-GFP⁺⁺* epicardial-enriched cells at different stages of embryonic heart development

We focused our attention on *Wt1GFP⁺⁺* epicardial-enriched cells and analysed their expression profile at different stages of heart development. We chose a time period that spanned the early formation of the epicardium, epicardial EMT, and a stage at which the heart had achieved an almost prenatal configuration (Miquero and Kelly, 2013). qRT-PCR analysis confirmed that during this time period there is a downregulation of *Wt1* gene expression in the *Wt1GFP⁺⁺* cells (Fig. S1B). Briefly, RNA from *Wt1GFP⁺⁺* sorted epicardial-enriched cells from heart ventricles were isolated each day from E11.5 to E16.5 (Fig. 2A,B) and used for the transcriptomic analysis (see Materials and Methods).

Using variance analysis, we identified a total of 1157 transcripts for which expression changes were statistically significant and took

place during more than two of the stages analysed. A hierarchical clustering of these 1157 modulated transcripts demonstrated four distinctive behavioural patterns summarised under Clusters 1 to 4 (Fig. 2C).

Although *Wt1^{GFP}* mice are not lineage-tracing mice, the stability of the GFP in the *Wt1GFP⁺⁺* population allowed us to identify all important sequential transitions in this dataset that take place during epicardial development (Fig. 2C). Cluster 1 contains genes that are highly expressed during the early stage of epicardial formation (E11.5 to 12.5) and are then progressively repressed (E13.5 onwards). Cluster 2 contains genes for which expression is low during the first two time points (E11.5 to 12.5) and for which regulation begins to increase from E13.5 onwards. Cluster 3 contains genes for which expression also begins to increase at E13.5, peaks at E14.5 and is then downregulated. Finally, Cluster 4 includes genes with maximum expression from E15.5 to 16.5 (Fig. 2C).

Each cluster analysed includes genes with biological functions that are relevant for the stage-dependent transcriptional changes that take place during epicardial development. Epicardial maturation and differentiation genes were over-represented in three clusters

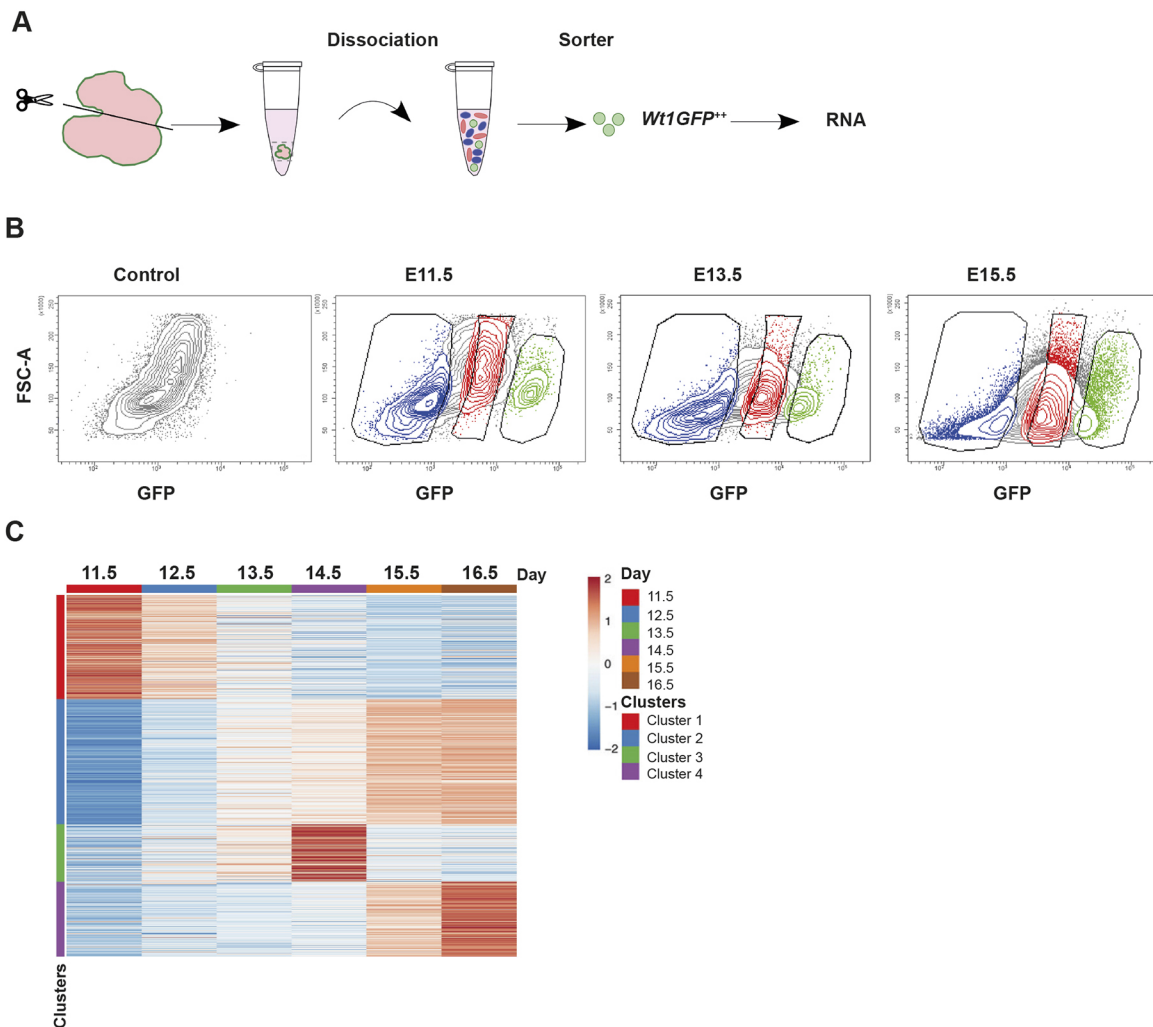


Fig. 2. Dynamic transcriptional signatures of epicardial development. (A) Schematic of *Wt1GFP⁺⁺* isolation of cells from embryonic hearts at different days of heart development. (B) FACS analyses of enzymatically digested hearts from *Wt1GFP* mice at the indicated stages of development. A plot of a negative-control GFP littermate (E11.5) heart is also shown. Two distinct types of *Wt1GFP*-positive cells are observed as indicated in Fig. 1. (C) Identification of the embryonic epicardial programme. Heatmap for the hierarchical clustering of the gene expression profiles of *Wt1GFP⁺⁺* cells at different days of heart development. Samples were quantiles normalised in R; statistical differences were assessed by ANOVA, with the false discovery rate based on permutations, $P < 0.05$. Red represents high gene expression and blue low gene expression. RNA from isolated cells from at least ten embryonic hearts was pooled by embryonic stage to make one replicate. Three replicates per stage were used for the analysis.

(Clusters 1, 2 and 4), whereas genes included in Cluster 3 could be representative of epicardial EMT.

Cluster 1 contained genes that regulate the cell cycle, such as *Ccnd2* and *Cdk4* (Table S2, Fig. S2A). The expression pattern of these genes correlates with previous reports in which the early stages of the epicardium show the highest proliferation rate (Wu et al., 2010). A series of cell adhesion molecules, including *Podxl*, *Alcam*, *Cdh3* and *Itga3*, was also represented in this cluster, thus implying an extensive adjustment of cell adhesion properties in the embryonic epicardium.

Cluster 2 contains genes that have previously been identified in the epicardium, including *Cav1*, *Fos*, *Meox1*, *Notch1*, *Hes1*, *Notch4*, *Nrarp* and *Nfatc1* (Table S2, Fig. S2A). In addition, some have also been shown to play a crucial role in epicardial development (Cao et al., 2016; Combs et al., 2011; del Monte et al., 2011).

Genes included in the transient Cluster 3 could be representative of the final steps of epicardial EMT or the transcriptomic profile of EPDCs (Table S2, Fig. S2A). This cluster demonstrates that *Wt1GFP⁺⁺* cells undergo a transitory change characterised by an increase in the expression of extracellular matrix (ECM) proteins, including *Col2a1*, *Des* and *Emilin1*, and an increase in the expression of cell adhesion molecules such as *Itgb5*, *Ncam1*, *Vcam1* and *Vcan* (Table S2, Fig. S2A). Interestingly, some of these molecules have previously been associated with EMT or cell migration in other cellular contexts (Bianchi et al., 2010; Lehembre et al., 2008; Wang et al., 2014a).

Cluster 4 is highly enriched with genes that belong to the insulin-like growth factor-binding family of proteins, IGFBP (Table S2), which could suggest that this family of proteins plays an important role in cell growth, cell differentiation and survival of the epicardium (Firth and Baxter, 2002). We also observed the presence of genes such as *Msln*, *Cldn15*, *Dmkn*, *C2*, *C3*, *Prr15*, *Slc9a3r1*, *Muc16* and *Igfbp6*, which have previously been described in the adult epicardium (Table S2, Fig. S2A) (Bochmann et al., 2010).

Two genes from each cluster were selected for validation and analysed for expression by qRT-PCR using *Wt1GFP⁺⁺* sorted cells. The genes confirmed the expression patterns found in the microarray (Fig. S2A). Two genes from each cluster were also validated by *in situ* hybridisation, which further corroborated the gene-selective epicardial expression (Fig. S2B). We also analysed the expression pattern of around 20 genes using the Euxpress database (www.euxpress.org); a list containing the links for these genes in the database is given in Table S3).

This dataset demonstrates the dynamic gene expression profile of *Wt1GFP⁺⁺* epicardial-enriched cells during different stages of heart development. Furthermore, based on the results presented here, this transcriptomic profile could be considered the embryonic epicardial programme.

Effect of *Wt1* loss on the molecular signature of *Wt1GFP⁺⁺*-enriched epicardial cells

Next, we decided to analyse the role of *Wt1* in this signature, so we compared the transcriptomic profile of *Wt1GFP⁺⁺* enriched epicardial cells from control and *epiWt1KO* mice at E13.5 (Fig. 3A). In these mice, one allele of *Wt1* is a conditional allele whereas the other allele is a GFP knock-in; efficient deletion of the *Wt1* gene in the epicardium was already observed at E11.5 (Martinez-Estrada et al., 2010). This strategy enabled us to use FACS to isolate epicardial-enriched cells from control mice (*Gata5^{Cre+}; Wt1^{loxP/GFP}*) and from *epiWt1KO* mice (*Gata5^{Cre+}; Wt1^{loxP/GFP}*) (Fig. 3A, Fig. S3A,B). Differential gene

expression analysis revealed 119 transcripts (100 known genes) with a statistically significant, at least twofold expression change (Fig. 3B, Table S4). The majority of the genes detected were upregulated in *epiWt1KO* and just 11 genes were downregulated in *epiWt1KO* (Table S4). A signature of *Wt1*-dependent genes was selected and confirmed by quantitative real-time PCR (Fig. S4A).

In order to elucidate the role of *Wt1* in the embryonic epicardial programme, we compared both gene expression profiles. Out of 100 unique genes modulated in the *epiWt1KO* epicardium, 41 (47 transcripts) were also modulated during the time-course experiment (Figs 3C and 2C), segregated as follows: 37% in Cluster 1, 17% in Cluster 2, 7% in Cluster 3 and 39% in Cluster 4 (Table S5). Most were upregulated in *epiWt1KO* and just seven genes were downregulated in *epiWt1KO*. Interestingly, out of these seven downregulated genes, none belonged to Cluster 1, three belonged to Cluster 2, two to Cluster 3 and two to Cluster 4 (Table S5).

To further investigate cellular functions over-represented among the modulated genes, we performed a gene ontology (GO) enrichment analysis using STRINGdb software. We found *Bmp4* to be one of the main genes enriched in two important categories related to tissue development: tissue morphogenesis and regulation of the cellular response to growth factor stimulus (Fig. S4B).

BMP4 signalling plays an important role during the formation of several tissues. Its wide range of functions is controlled in part by inhibitors that impede the interaction between BMP4 and its specific receptors; BMP4 expression and inhibition are therefore both crucial for many developmental events (Zhao, 2003). Our transcriptomic analysis indicated that *Bmp4* belongs to Cluster 1 and is upregulated in the *epiWt1KO* epicardium. Interestingly, its antagonist *Nb11* (neuroblastoma suppressor of tumorigenicity 1, also known as DAN), which prevents the interaction of BMP4 with its receptors, belongs to Cluster 4 and is downregulated in the *epiWt1KO* epicardium.

Collectively, these analyses reveal the role of *Wt1* in the regulation of the gene signature of *Wt1GFP⁺⁺* enriched epicardial cells and identify new genes potentially involved in epicardial development.

Wt1 is required for the epicardial flattening that takes place during maturation of the epicardium

BMP4 signalling activity has previously been linked to tissue morphogenesis events in which changes in cell shape have taken place (Nilsson and Skinner, 2003; Zhao, 2003). Next, we decided to examine the epicardial cell shape in *epiWt1KO* embryos using scanning electron microscopy (SEM) and transmission electron microscopy (TEM) (Fig. 4A). At E15.5, flattened epicardial cells were present in control hearts, whereas most *Wt1KO* epicardial cells presented a cuboidal cell shape (Fig. 4A). The quantification of epicardial cell length and aspect ratio (AR) in control versus knockout cells confirmed that the cell length and AR of mutants were reduced by 32% and 44%, respectively, whereas circularity in mutants increased by 60%, thus indicating that *Wt1* controls the degree of flattening of the epicardium (Fig. 4B).

We also analysed the morphology of the epicardium using immunofluorescence staining with podocalyxin and podoplanin together with sarcomeric myosin staining (MF20) to visualise the myocardium. Immunofluorescence staining of these proteins at E15.5 confirmed the flattened and elongated morphology of the control epicardium compared with the cuboidal shape of the epicardial cells from *epiWt1KO* mice (Fig. 4C).

We subsequently studied whether the persistence of the cuboidal cell shape in the epicardium of mutant mice is a result of an

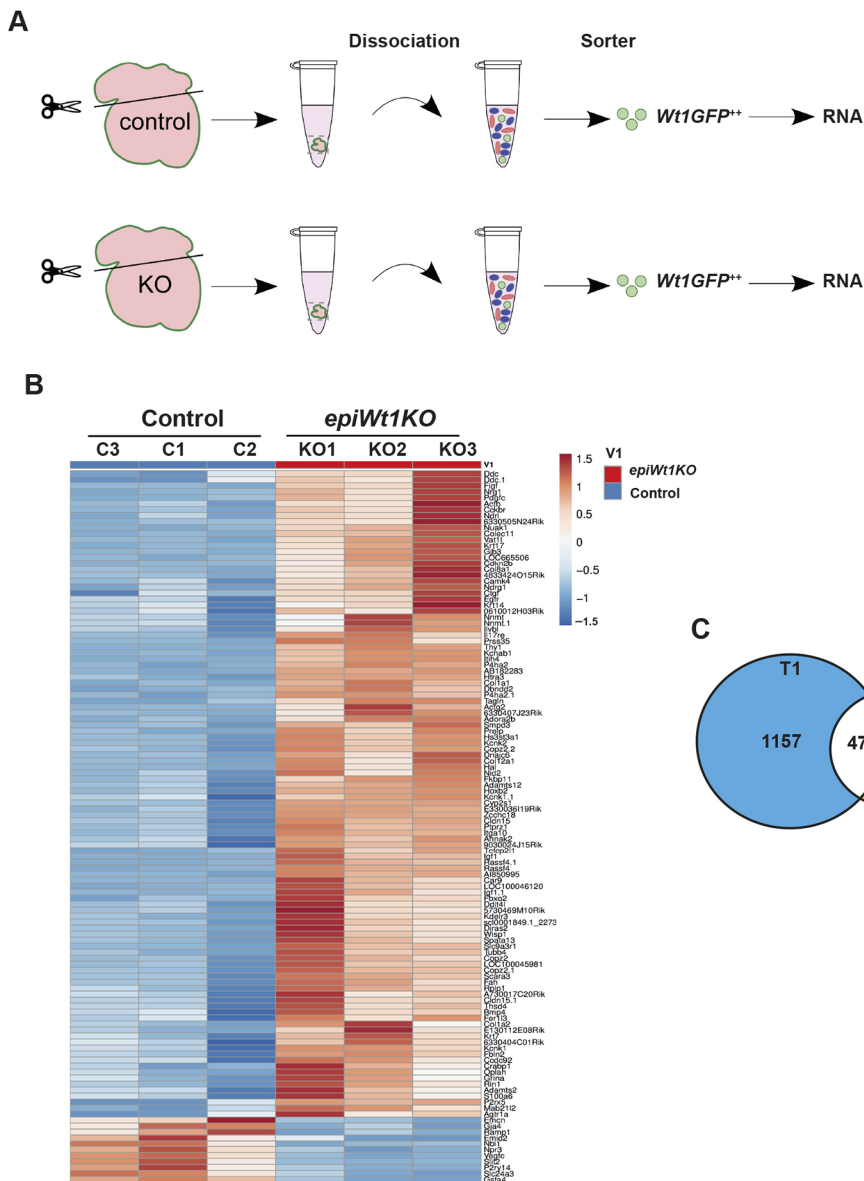


Fig. 3. Gene profiling of *Wt1GFP⁺⁺* sorted cells from control and *epiWt1KO* mice.

(A) Schematic of the *Wt1GFP⁺⁺* cell isolation procedure from control and *epiWt1KO* mice. (B) Heatmap of differentially expressed genes identified by microarray analysis in *Wt1GFP⁺⁺* FACS-sorted cells from E13.5 control and *epiWt1KO* mice. Transcripts regulated more than twice were considered significantly regulated. Statistical differences were assessed by *t*-test, with the false discovery rate 1%, $P < 0.05$. RNA from isolated cells from at least ten embryonic hearts was pooled to make one replicate, and three replicates per condition were used for the analysis. (C) Identification of the role of *Wt1* in the embryonic epicardial programme. Venn diagram showing the overlap of dynamically modulated genes during epicardial development (T1) with genes modulated in *Wt1GFP⁺⁺* epicardial cells from *epiWt1KO* mice (T2).

impairment in the cell shape change that may occur during the epicardial maturation process. To explore this biology, we carefully analysed the heart surface of embryonic mice at different developmental stages using SEM and TEM (Fig. 4D). At E11.5, the stage when the whole myocardial surface is first covered by the epicardium, epicardial cells present cuboidal properties, with large, centrally located nuclei, and by E13.5 epicardial cells begin to elongate (Fig. 4D). This increase in cell length correlates with an increase in AR, a measure of the degree to which flattening has occurred, and a decrease in circularity (Fig. 4E). As the heart development process continues, the epicardium continues to elongate and stretch, and epicardial cells become even more flattened by stage E15.5, thus giving rise to a squamous epicardium that is already present at E18.5 (Fig. 4D). This morphogenetic switch is completed by the appearance of a flattened nucleus, which is present in the more mature epicardium (Fig. 4D).

To further confirm these findings, we also analysed the morphology of the epicardium at different stages of development using immunofluorescence staining with podocalyxin and podoplanin. At the early stages of epicardial development,

podocalyxin and podoplanin staining confirmed the cuboidal morphology of epicardial cells; as epicardial development proceeds, the flattened or squamous morphology of epicardial cells is clearly observed (Fig. 4F, Fig. S5A). Interestingly, one of the notable features of this cuboidal primitive epicardium is its unpolarised phenotype characterised by the apical and lateral localisation of podocalyxin, which is very similar to the distribution of this protein in the mutant mice (Fig. 4C,F).

To examine the functional significance of this cell arrangement, we used Sulfo-NHS-LC-Biotin to compare epicardial permeability in the early stage versus the mature stage (Fig. S5B). In E18.5, biotin staining of the hearts was confined to the epicardial layer, in contrast to E11.5 embryonic hearts, where biotin was also detected in the myocardium (Fig. S5B). These findings strongly suggest that epicardial maturation induces a reorganisation of cell-cell junctions.

Taken together, these data indicate that deletion of *Wt1* in the epicardium impairs the maturation process of the primitive epicardium, which is characterised by a cuboidal-to-squamous transition that induces the formation of a less permeable mature epicardium.

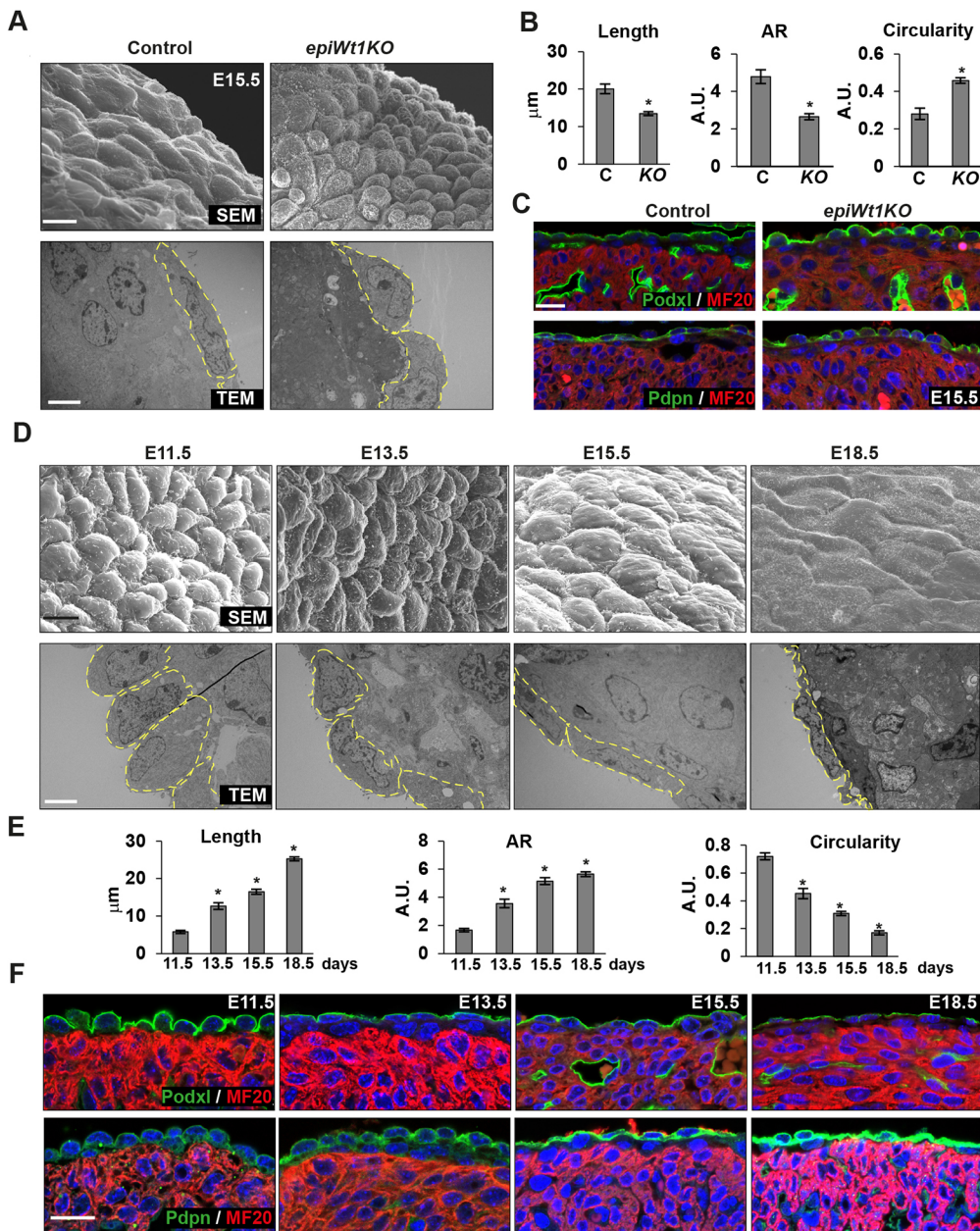


Fig. 4. Loss of *Wt1* inhibits epicardial flattening. (A) Representative SEM and TEM images of epicardial cells from control and *epiWt1KO* at E15.5 days of development. (B) Quantification of epicardial cell length, aspect ratio (AR) and circularity in control ('C') and *epiWt1KO* ('KO') heart ventricles are shown as mean \pm s.e.m. Three independent embryos were assessed per condition, and at least 25 epicardial cells were quantified. Significance was determined by two-tailed *t*-tests ($*P < 0.05$). (C) Heart sections from control and *epiWt1KO* E15.5 embryos were stained for podocalyxin (Podxl) and podoplanin (Pdpn) (green), MF20 (red) and nuclear Hoechst stain (blue). (D) SEM and TEM of the epicardium at different days of heart development indicating changes in epicardial cell shape. (E) Quantification of epicardial cell length, AR and circularity at different days of heart development is shown as mean \pm s.e.m. Three independent embryos were assessed and at least ten epicardial cells were quantified. Significance was determined by Tukey's multiple-comparison after one-way ANOVA ($*P < 0.05$). (F) Immunofluorescence analysis of podocalyxin (Podxl), podoplanin (Pdpn) (green), MF20 (red) and nuclear Hoechst stain (blue) in heart sections at different days of development. In A and D, yellow dashed lines outline the shape of the epicardial cells. Scale bars: 10 μm (A, D, SEM); 5 μm (A, D, TEM); 20 μm (C, F).

***Wt1* regulates BMP4 signalling during epicardial development**

Next, we decided to investigate the molecular mechanism underlying *Wt1*-regulated epicardial cell maturation. GO enrichment analysis demonstrated that *Bmp4* is one of the main genes enriched in categories related to tissue development. Interestingly, *Bmp4* belongs to Cluster 1 and is upregulated in the *epiWt1KO* epicardium. We confirmed the dynamic expression of *Bmp4* and its antagonist *Nb1l* during different stages of heart development in *Wt1GFP⁺* sorted epicardial enriched cells by qRT-PCR (Fig. 5A,D). We observed that the BMP pathway is tightly regulated during epicardial maturation and is inversely correlated with cuboidal cell shape (Figs 5A-E and 4). The early stage is characterised by high expression levels of *Bmp4* and low expression levels of *Nb1l*, whereas the reverse expression pattern is present at the mature stage (Fig. 5A,D).

We also analysed the expression of *Bmp4* and *Nb1l* in *Wt1GFP⁺* sorted epicardial cells from control and *epiWt1KO* mice (Fig. 5B,E).

We observed an increase in the expression of *Bmp4* and a decrease in the expression of *Nb1l* in *epiWt1KO* epicardial cells, thus confirming that the BMP signalling pathway is tightly regulated by *Wt1* (Fig. 5B,E). In addition, RNAscope for *Bmp4* was performed on heart sections from control and *epiWt1KO* embryos (Fig. 5C). The RNAscope data demonstrated the specific expression of *Bmp4* in the epicardium and also confirmed the increased expression observed by qRT-PCR in the epicardial-enriched sorted cells.

Characterisation of *Wt1* binding using ChIP-on-chip and ChIP-seq in nephron progenitor cells during renal development has identified *Bmp4* as a *Wt1* target (Hartwig et al., 2010; Motamedi et al., 2014). Next, we decided to explore whether *Wt1* could directly bind to the *Bmp4* regulatory region in epicardial cells. ChIP experiments with an antibody against *Wt1* indicated that *Wt1* occupies the *Bmp4* regulatory region in epicardial cells (Fig. 5F).

Activation of the BMP4 canonical pathway is characterised by the phosphorylation of Smad1/5/8 (Wang et al., 2014b). In the

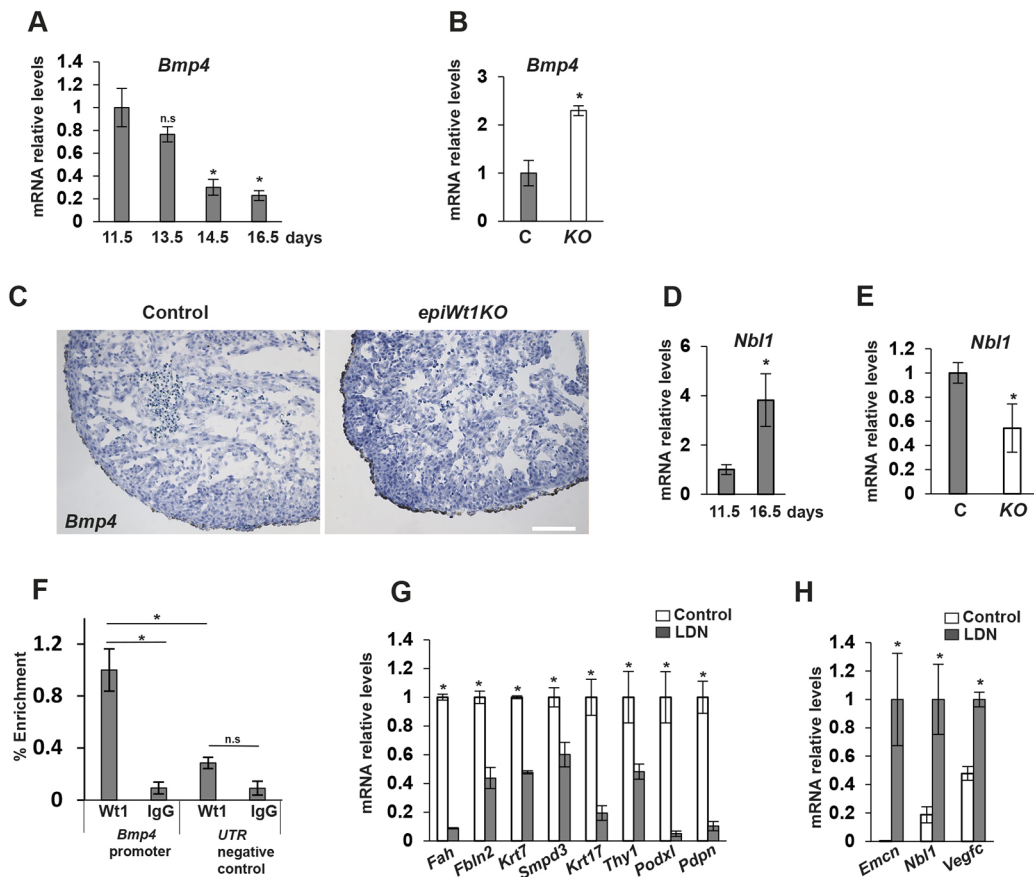


Fig. 5. Wt1 regulates BMP4 signalling during epicardial development. (A,B) qRT-PCR analysis of *Bmp4* expression in *Wt1^{GFP}*⁺ FACS-sorted epicardial cells from *Wt1^{GFP}* mice at different days of development (A) and in *Wt1^{GFP}*⁺ epicardial cells from control and *epiWt1KO* ventricles at E13.5 (B). Values represent mean \pm s.e.m., * P <0.05, one-way ANOVA followed by Tukey's post-hoc test (A) and two-tailed Student's *t*-test (B). (C) RNAscope *in situ* hybridisation analyses of *Bmp4* in hearts from control and *epiWt1KO* at E13.5. (D,E) qRT-PCR analysis of *Nbl1* expression in *Wt1^{GFP}*⁺ FACS-sorted epicardial cells from *Wt1^{GFP}* mice at indicated days of development (D) and in *Wt1^{GFP}*⁺ epicardial cells from control and *epiWt1KO* ventricles at E13.5 (E). (F) Wt1 binding to a *Bmp4* regulatory region was examined by ChIP with a Wt1 antibody and control IgG using immortalised epicardial cells. (F) Quantitative PCR of the immunoprecipitated DNA was conducted using primers flanking the Wt1 binding site and a 3'UTR region as a negative control. Values represent mean \pm s.e.m., * P <0.05, n.s., not significant, one-way ANOVA followed by Tukey's post-hoc test. (G,H) E11.5 *Wt1^{GFP}* hearts were cultured in the presence or absence of LDN-193189 (LDN) for 24 h. qRT-PCR analyses of indicated genes in *Wt1^{GFP}*⁺ sorted enriched epicardial cells from control and LDN-193189-treated hearts. Values represent mean \pm s.e.m., * P <0.05, two-tailed *t*-tests. RNA from FACS-isolated cells from at least ten embryonic hearts was pooled to make one replicate. Three replicates per condition were used for the analysis. Scale bar: 100 μ m.

epicardium, BMP4 activated the canonical BMP4/pSMAD pathway, as indicated by the increased expression of pSMAD1/5 (Fig. S6A). Next, we decided to investigate the role of *Bmp4* signalling in the transcriptional signature of the embryonic epicardium in greater depth. We examined the expression of selected genes for which expression is upregulated or downregulated in the *epiWt1KO* epicardium, respectively, and that have been previously modulated after the loss of Bmp signalling (Genander et al., 2014). Thus, we FACS-sorted *Wt1^{GFP}*⁺ enriched epicardial cells from *Wt1^{GFP}* hearts cultured in the presence or absence of the BMPRI inhibitor LDN-193189, which blocks Smad1/5 phosphorylation in epicardial cells (Fig. S6B). Additionally, we carried out qRT-PCR that showed that the inhibition of BMP signalling by LDN-193189 resulted in the decreased expression of Cluster 1 genes for which expression is upregulated in the *epiWt1KO* epicardium, including *Fah*, *Fbln2*, *Smpd3*, *Krt7* and *Podxl*, and an increase in the expression of Cluster 2 and Cluster 4 genes for which expression is downregulated in the epicardial cells from *epiWt1KO*, including *Emcn* and *Nbl1* (Fig. 5G, H). We also observed how the inhibition of BMP signalling

modulated other genes that are differentially expressed in the epicardial enriched cells from *epiWt1KO*, including *Krt17*, *Thy1* and *Vegfc* (Fig. 5G,H). Interestingly, we found that the inhibition of BMP signalling increases *Nbl1* expression, which may explain the inverse correlation of *Bmp4* and *Nbl1* during epicardial development and in *epiWt1KO* mice.

Together, these data indicate that Wt1 tightly regulates BMP4 signalling during epicardial development. These findings also suggest that the persistent BMP4 signalling in the epicardial cells from *epiWt1KO* plays a role in the regulation of several differentially expressed genes in the mutant epicardium.

Inhibition of BMP4 signalling rescues the flattening defects in *epiWt1KO* hearts

In view of the observation that a higher level of *Bmp4* correlates with the cuboidal cell shape of epicardial cells (Figs 4 and 5), we decided to test whether *Bmp4* is involved in the regulation of epicardial cell morphology. We therefore examined the effect of recombinant BMP4 on immortalised epicardial cells. Confocal imaging analyses of β -catenin staining demonstrated a uniform

staining pattern at the cell-cell contact and, interestingly, cell elongation, measured by AR, was found to be markedly lower in BMP4-treated cells (Fig. 6A).

Next, we decided to modulate the BMP4 signalling pathway in early developmental stages at which epicardial cells display a cuboidal morphology. We subsequently treated pregnant mice with LDN-193189, which has previously been used to inhibit BMP4 signalling *in vivo* (Yu et al., 2008). In order to demonstrate that maternal LDN-193189 treatment is effective in suppressing BMP4

signalling, western blot analyses of p-Smad1/5 were performed on embryonic hearts from control and LDN-193189-treated pregnant mice (Fig. S6C). Our western blot results demonstrated that LDN-193189 effectively reduced BMP4 signalling in the embryonic hearts.

We observed that LDN-193189 treatment did not impair epicardial formation, even when it was applied prior to formation, at the proepicardial stage (E9.5, see Materials and Methods for details). However, it did induce a change in cell morphology in the early

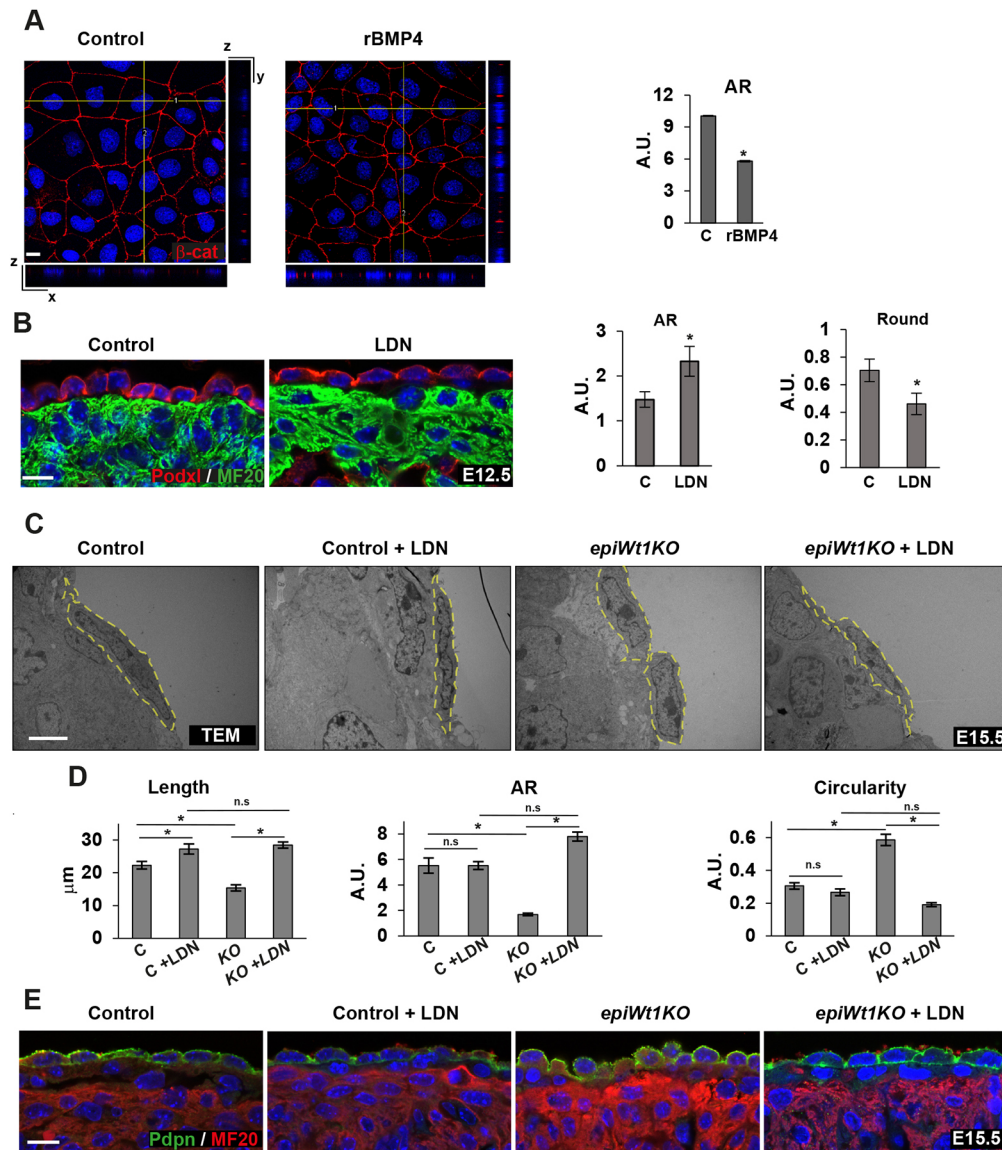


Fig. 6. BMP4 signalling is involved in the maintenance of the cuboidal phenotype of epicardial cells. (A) Confocal immunofluorescence analysis of beta-catenin (β -cat) in epicardial cells cultured in the presence of recombinant BMP4 (rBMP4). Orthogonal xz and yz projections of 3D confocal image stacks of epicardial cells stained for β -cat (red) and DAPI (nuclei, blue) are shown to illustrate the morphology of the cells. Graph shows quantification of epicardial cell AR in immortalised epicardial cells cultured in the presence of rBMP4. At least 35 cells were analysed per condition in four independent experiments. Error bars represent \pm s.e.m. and P -values are based on two-tailed t -tests ($*P < 0.05$). (B) E12.5 heart sections from control and LDN-193189-treated (LDN) embryos were stained for podocalyxin (red), MF20 (green) and nuclear Hoechst stain (blue). Pregnant mice were injected with control vehicle or LDN-193189 by E9.5-E12.5 days of pregnancy. Quantification of epicardial cell AR and round shape are shown. Error bars represent \pm s.e.m. and P -values are based on two-tailed t -tests ($*P < 0.05$, $n = 3$). (C) TEM of control and *epiWt1KO* hearts at E15.5 from pregnant mice injected by days E13.5-E15.5 with control vehicle or LDN-193189 (LDN), indicating that flattening was rescued in epicardial *epiWt1KO* cells in the presence of LDN. Yellow dashed lines outline the shape of the epicardial cells. (D) Quantification of epicardial cell length, AR and circularity are shown as mean \pm s.e.m. Three independent embryos were assessed per condition, and at least 20 epicardial cells were quantified. Significance was determined by Tukey's multiple-comparison after one-way ANOVA ($*P < 0.05$, n.s., not significant). (E) Immunofluorescence analysis of podoplanin (green), MF20 (red) and nuclear Hoechst stain (blue) in heart sections of control and *epiWt1KO* hearts at E15.5 from pregnant mice injected with control vehicle or LDN-193189 (LDN) as indicated above. Scale bars: 10 μ m (A); 20 μ m (B,E); 5 μ m (C).

cuboidal epicardial cells towards a more flattened phenotype, which correlates with an increase in AR and a decrease in the rounded shape (Fig. 6B). We also found that LDN-193189 treatment did not induce gross change in heart morphology (Fig. S6E).

We decided to use both an *ex vivo* and an *in vivo* approach to further examine whether BMP4 upregulation contributes to the flattening defects observed in the *epiWt1KO* epicardium. Firstly, control and *epiWt1KO* hearts were cultured in the presence of dorsomorphin, a BMP4 pathway inhibitor that also reduces pSmad1/5 in epicardial cells (Fig. S6D). TEM analyses of dorsomorphin-treated *epiWt1KO* hearts demonstrated that BMP4 pathway inhibition rescued the flattened epicardial morphology (Fig. S6F,G). We then treated pregnant mice carrying control and mutant mice with LDN-193189 at E13.5 (see Materials and Methods). We observed that LDN-193189 treatment was sufficient to rescue the *epiWt1KO* cuboidal phenotype 48 h later. TEM analyses of LDN-treated *epiWt1KO* hearts demonstrated that *Wt1KO* epicardial cells lost their cuboidal morphology and became flatter, with elongated nuclei (Fig. 6C,D). Interestingly, the rescue of the epicardial morphology also correlates with a rescue in the localisation of podoplanin, which adopted a cellular distribution similar to that seen in the control epicardium (Fig. 6E).

Together, these data indicate that the upregulation of the *Bmp4* signalling pathway in the *Wt1KO* epicardium is responsible for the maintenance of a cuboidal phenotype in the mutant epicardium.

Bmp4 downregulation also correlates with lung mesothelial maturation

The mechanisms underlying visceral mesothelial cell maturation are virtually unknown. Next, we decided to analyse whether similar changes in cell morphology happen during lung mesothelial maturation. Both TEM and immunostaining analysis of developing lungs demonstrated that lung mesothelial cells present cuboidal properties at E12.5, and the mature mesothelium has already adopted a squamous or flattened phenotype by E18.5 (Fig. 7A,B). We then analysed the expression of *Bmp4* in *Wt1-GFP* sorted mesothelial cells from developing lungs at different stages of development (Fig. 7C). We observed that the formation of the mature lung mesothelium also correlates with a decrease in the expression of *Bmp4* levels. In addition, we observed a reduction in the expression of early genes, such as *Podxl*, *Tbx18* and *Wt1*, and an increase in the expression of *Msln*, a mature gene found in Cluster 4, thus confirming the mesothelial nature of these cells.

Taken together, these data indicate that, as with the epicardial morphogenesis, the maturation of the lung mesothelium is

characterised by a cuboidal-to-squamous transition that inversely correlates with *Bmp4* expression levels.

DISCUSSION

Despite the importance of the epicardium in heart development and repair, a transcriptomic profile that interrogates the cellular dynamics and functions of the epicardium during different stages of heart development remains elusive. Here, we provide a comprehensive analysis of the transcriptome of *Wt1GFP⁺⁺* enriched epicardial cells during different stages of heart development. In addition, in order to identify the role of *Wt1* in this signature, we also compared the transcriptomic profile of *Wt1GFP⁺⁺* epicardial enriched cells from control and *epiWt1KO* mice. One of the main findings of these analyses, in conjunction with cellular morphology and functional analyses, is the crucial role of *Wt1* in the transition between the cuboidal and the flattened cell shape that characterises epicardial maturation, a process that leads to the formation of a squamous, less permeable epicardium.

We identified *Bmp4* as a transcriptional target of *Wt1*, thus providing a molecular basis for the retention of the cuboidal cell shape observed in the epicardium of *epiWt1KO* mice. Furthermore, the rescue of the mutant phenotype by inhibition of BMP4 signalling, both *ex vivo* and *in vivo*, proves that *Wt1* is vital for epicardial maturation through the direct repression of *Bmp4* and its downstream pathway.

Epicardial maturation: a process regulated by Wt1

Changes in cell shape, from cuboidal to flattened, are crucially important for the formation of squamous epithelia during tissue morphogenesis (Gomez et al., 2012; McClure and Schubiger, 2005). It has been proposed that, once proepicardial cells reach the myocardium surface, they become flattened and spread out; however, a detailed characterisation of this transition from both a cellular and a functional point of view has not been produced so far (Komiyama et al., 1987). Here, we performed detailed morphological and functional analyses of the embryonic epicardium during different stages of heart development and showed that epicardial maturation is characterised by a change in cell shape, from cuboidal in early epicardial development to squamous in the later stages. Our results also suggest that the maturation of the epicardium induces junction remodelling and, as a consequence, the formation of a mature, squamous, less-permeable epicardium.

Mature tissues arise through highly controlled cell differentiation mechanisms. Recent studies have identified new functions for *Wt1* in several aspects of epicardial biology (Hastie, 2017); however, the

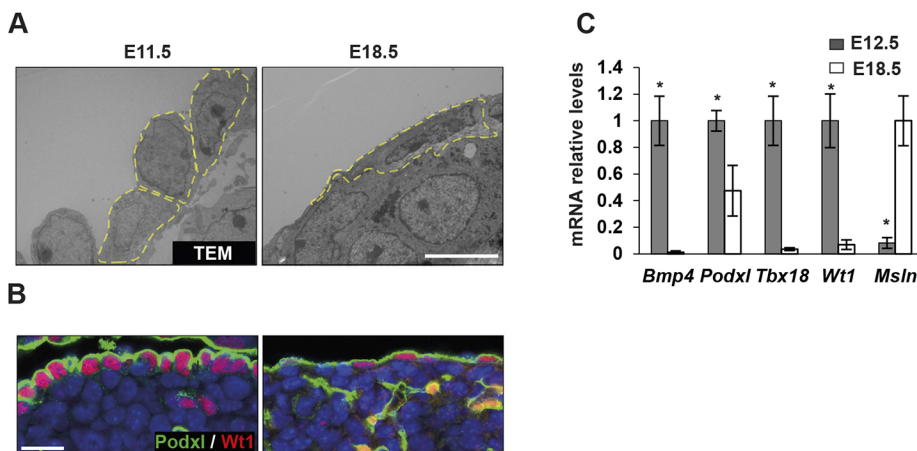


Fig. 7. *Bmp4* expression inversely correlates with a cuboidal-to-squamous transition during lung mesothelial maturation.

(A) Representative TEM of lung sections at E11.5 and E18.5. Yellow dashed lines outline the shape of the epicardial cells.

(B) Immunofluorescence staining for *Wt1* (red), podocalyxin (green) and nuclear Hoechst stain (blue), in lung sections at the indicated stages.

(C) qRT-PCR analyses of the indicated genes in *Wt1GFP* sorted mesothelial cells at different days of development. Values represent mean \pm s.e.m. and *P*-values are based on one-tailed *t*-tests.

**P* < 0.05, *n* = 3. Scale bars: 5 μ m (A); 20 μ m (B).

role of this protein in epicardial maturation has not previously been explored. Here, we report the transcriptomic profile of *Wt1GFP⁺⁺* epicardial enriched cells during different stages of development, and also of *Wt1GFP⁺⁺* epicardial enriched cells from control and *epiWt1KO* mice. Transcriptomic and cellular morphology analyses demonstrated a defect in the maturation process of the mutant epicardium. Two key findings from our transcriptomic analyses, relevant for the regulation of epicardial cell shape, are the reduction in *Bmp4* expression, as epicardial cells mature from a cuboidal to a squamous shape, and the upregulation of *Bmp4* in the *epiWt1KO* epicardium, which has a cuboidal morphology (Fig. 8). We identified *Bmp4* as a transcriptional target of *Wt1*, thus providing a molecular basis for the retention of the cuboidal cell shape observed in the *Wt1KO* epicardium. Accordingly, the inhibition of the BMP4 signalling pathway both *ex vivo* and *in vivo* rescued the *epiWt1KO* cuboidal phenotype. Our inhibition experiments also demonstrated that *Bmp4* signalling is able to modulate the expression of several genes differentially modulated in the *epiWt1KO*. Which of these genes or combination of genes are directly involved in the regulation of epicardial cell shape remains to be determined.

Several Cre drivers, including *Gata5^{Cre}*, *Tbx18^{Cre}*, *Wt1^{GFP^{Cre}}*, *Wt1^{Cre}*, *Wt1^{CreERT2}* and *Sema3a^{GFP^{Cre}}*, have been used in recent years to study the role of different genes in epicardial development (Baek and Tallquist, 2012; del Monte et al., 2011; Singh et al., 2016; Wu et al., 2010; Zamora et al., 2007). Unfortunately, a Cre driver with such restricted epicardial specificity does not exist. The *epiWt1KO* mouse model analysed in this study was generated using

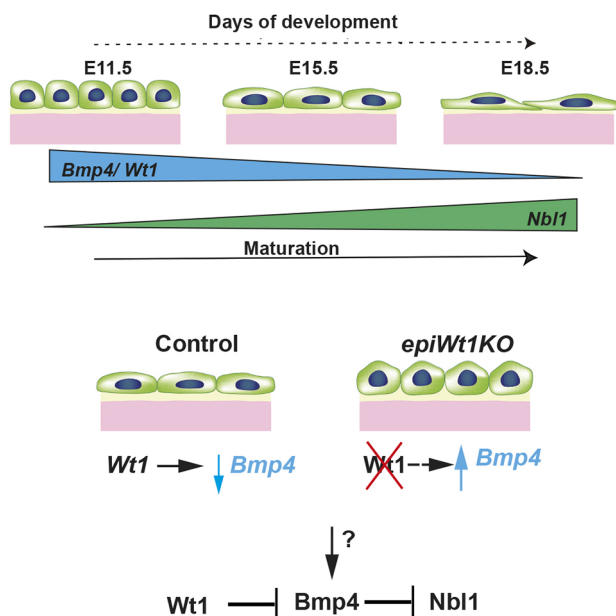


Fig. 8. Model of the cuboidal-to-squamous transition process that takes place during epicardial maturation. During embryonic heart development, epicardial cells undergo a change in cell shape from a cuboidal to a flattened phenotype to form a mature squamous epicardium. The epicardium maturation process inversely correlates with *Bmp4* expression levels. *Bmp4* expression in the epicardium is repressed by *Wt1* and can therefore orchestrate the transition from a cuboidal to a squamous morphology, which is affected in *epiWt1KO* mice. Inhibition of BMP signalling increases *Nb11* expression, which may explain the inverse correlation of *Bmp4* and *Nb11* during epicardial development and in *epiWt1KO* mice. The transcriptional activator(s) and signalling pathway(s) that modulate the expression of *Bmp4* in the epicardium and are probably downregulated over the course of epicardium maturation remain unidentified.

the *Gata5^{Cre}* driver. Despite the putative caveats of our model, our article offers several pieces of evidence that support the epicardial specificity of our findings. We observed an inverse correlation of *Bmp4* levels during normal epicardial development and found that the maturation process of the embryonic epicardium is characterised by the acquisition of a squamous phenotype. In addition to *in vivo* approaches, we also performed *in vitro* experiments with immortalised epicardial cells. These experiments strongly support our findings and demonstrate the role of *Bmp4* in the regulation of epicardial cell shape. In addition, it also indicates that the cuboidal phenotype observed in *epiWt1KO* is unlikely to be generated by the activation of the *Gata5^{Cre}* in other heart components.

The persistence of a primitive cell shape in the epicardium can also be observed in other mutant mice with an epicardial development defect; however, this phenotype has not been linked to a defect in the maturation process (Tran et al., 2016; Xiao et al., 2018). In this regard, an increase in the number of cells with round nuclei has been described in *Lb1 (Ckap2)* null mice (Tran et al., 2016). Interestingly, the cell shape changes that characterise epicardial maturation also imply a change in nuclear morphology, as observed in our morphological analysis.

The BMP4 signalling pathway has been implicated in the development of the proepicardium in zebrafish and chick embryos (Ishii et al., 2010; Kruthof et al., 2006; Liu and Stainier, 2010; Schlueter et al., 2006); however, little is known about the role of this pathway in the mammalian epicardium (Lockhart et al., 2014). Accurate levels of *Bmp4* signalling are crucial during organ development (Wang et al., 2014b). Here, we demonstrate that *Wt1* is a repressor of the *Bmp4* gene in the embryonic epicardium. In addition, we also demonstrate that *Bmp4* modulates the levels of its antagonist *Nb11*. One question that remains unanswered is which transcriptional activator(s) or positive signalling pathways modulate *Bmp4* expression in epicardial development? We hypothesised that such activator(s) or positive signalling pathways should be also downregulated during the course of epicardial formation; this is a plausible explanation for why the reduction in *Wt1* during normal embryonic development is not also linked to an increase in *Bmp4* expression (Fig. 8).

A recent analysis of the embryonic pancreatic mesothelium was reported using single cell sequencing of the embryonic pancreas (Byrnes et al., 2018). As with our analysis of the epicardium, the early stage of the pancreatic mesothelium was characterised by high expression levels of *Bmp4*, whereas the mature stage displayed high expression levels of *Nb11*.

The transcriptomic profile of *Wt1GFP⁺⁺* cells: identifying novel genes and pathways involved in different aspects of epicardial development

The identification of the gene expression profile of a population of cells during different stages of organ development can provide important insights into their main morphogenetic and functional changes. Here, we identified the transcriptomic profile of *Wt1GFP⁺⁺* epicardial-enriched cells during different stages of heart development. The stability of the GFP protein in *Wt1GFP⁺⁺* cells made it possible to create a profile of epicardial cells during the early stage of epicardial development, epicardial EMT and the maturation and differentiation of epicardial cells.

Our profiling recapitulated genes known previously to be expressed in the epicardium, but it also identified a large number of new genes that can be used as markers for each developmental stage. Some of these new genes, in a similar way to *Wt1* and *Raldh2*, will be switched on in the adult epicardium following MI (van Wijk

et al., 2012; Zhou et al., 2011). In this regard, we hypothesise that, as with zebrafish, the reactivated mammalian epicardium will switch on the expression of BMP4 following MI, which will induce the presence of a cuboidal proliferating phenotype and the re-expression of early epicardial genes (Cao et al., 2016).

One intriguing finding of our analysis is the presence of some genes in Cluster 2 that are usually abundantly expressed in endothelial cells (ECs), and are consequently considered to be endothelial specific. As a low percentage of *Wt1*-positive cells has been reported to contribute to the coronary endothelium, we cannot rule out the possibility of a low contamination of *Wt1*-positive ECs in our study (Cano et al., 2016; Dube et al., 2017; Sharma et al., 2017; van Wijk et al., 2012; Zhou et al., 2008). An unbiased classification of epicardial cell types using single cell transcriptomics would help clarify this finding.

Revealing marker genes for EPDCs

Although a large body of literature supports the contribution of epicardial EMT to the formation of EPDCs, the main molecular features of this transition remain elusive. Genes belonging to Cluster 3 transiently increase their expression between E13.5 and E14.5, which correlates with the expansion of EPDCs. Whether this change in gene expression represents the final steps of epicardial EMT or the transcriptomic profile of at least one subpopulation of EPDCs requires further investigation.

Despite the putative limitations of our study, given that we analysed the transcriptomic profile of a population of epicardial enriched cells, we believe that the gene profile data from this study constitute an excellent resource for identifying new genes and pathways that are involved in the different stages of epicardial development. Most of the single cell gene expression analyses that have been performed in the heart have completely overlooked the epicardium (Massaia et al., 2018). Identifying the modulation of genes expressed during the development of cardiac tissue is vital to our understanding of the role of these genes in its formation and even repair.

MATERIALS AND METHODS

Animal models

The *Wt1^{GFP}* mice and epicardial-specific *epiWt1KO* mice (*Gata5^{Cre+}; Wt1^{loxP/gfp}*) have been described previously (Hosen et al., 2007; Martínez-Estrada et al., 2010). Embryos were generated through timed matings, whereby females that have mated during the night are checked for plugs early the following morning. The morning on which a plug is found is considered to be E0.5. To generate *Wt1^{GFP}* embryos at different stages of development, *Wt1^{GFP}* mice were mated with CD1 mice. The *epiWt1KO* (*Gata5^{Cre+}; Wt1^{loxP/GFP}*) mice were generated by cross-breeding *Gata5^{Cre+}; Wt1^{GFP}* with *Wt1^{loxP/loxP}* mice. Genotyping was carried out using the primers listed in Table S6. At least five embryos were analysed for each stage and genotype. All animal experiments were carried out in accordance with regulations issued by the Home Office (MRC/UoE) and were approved by the Animal Welfare and Ethics Board (AWERB) of the University of Edinburgh and the Animal Experimentation Ethics Committee (CEEA) of the University of Barcelona, thereby complying with current Spanish and European legislation.

SEM and TEM

For SEM, embryonic hearts and lungs were fixed overnight (2% paraformaldehyde, 2.5% glutaraldehyde in 0.1 M cacodylate buffer), post-fixed for 2 h (1% osmium tetroxide, 0.8% potassium ferrocyanide in 0.1 M phosphate buffer) and subsequently processed as described in standard protocols. Images were taken on a JEOL JSM 7100F. For TEM, both organs were processed as described for SEM until post-fixation. Hearts were then dehydrated in a graded series of ethanol and transitioned into EPON resin.

The tissue was embedded in moulds containing fresh resin and polymerised for 2 days at 65°C. Sections 0.5 µm thick were stained with Methylene Blue to determine the area for thin sectioning (at 70 nm) with a diamond knife. Thin sections were placed onto formvar on 100-mesh copper grids and stained with aqueous uranyl acetate and lead citrate. The grids were examined using a Tecnai Spirit TWIN TEM (FEI) 120 kV LaB6 and CCD Megaview 1Kx1K digital camera.

Determination of cell shape parameters

The morphological parameters of cell shapes were measured using ImageJ (National Institutes of Health). Morphological analyses were performed as described previously (Trescos et al., 2015) and three parameters were calculated for each cell: length; circularity index ($4\pi \times \text{area}/\text{perimeter}^2$), which assumes values between 1 for a circular shape and 0 for an elongated morphology; and AR (length of major axis/length of minor axis), values of which become greater than 1 with increased elongation.

Immunohistochemistry

Mouse embryos were fixed in 4% paraformaldehyde (PFA), embedded in paraffin and sectioned. Antigen retrieval was carried out by boiling samples in a pressure cooker for 4 min in TEG buffer (10 mM Tris and 0.5 mM EGTA, pH 9.0). Slides were then incubated in 50 mM NH₄Cl in PBS (pH 7.4) for 15 min, then in blocking serum (Springbio, DPB-125) for 30 min, followed by overnight primary antibody incubation at 4°C. Slides were then washed with PBS, incubated at room temperature for 2 h with the appropriate secondary antibodies and nuclei stained with Hoechst 33342 (Thermo Fisher Scientific, 62249) for 15 min. For a list of all antibodies and dilutions used, see Table S7. Samples were imaged using an N-STORM Super-Resolution laser microscope (Nikon).

Epicardial cell culture

Immortalised epicardial cells were cultured and propagated in DMEM 4.5 g/l glucose, 10% fetal bovine serum (FBS) at 33°C (Guadix et al., 2011). For western blot analyses, 1.5×10^5 epicardial cells were seeded into 6-well plastic culture plates. After 18 h of incubation, the medium was changed to 2% FBS supplemented with either dorsomorphin (4 µM, Sigma-Aldrich) or LDN-193189 (0.5 µM, Sigma-Aldrich). For time-course analyses of BMP4, immortalised epicardial cells were pretreated for 18 h with dorsomorphin before BMP4 stimulation (100 ng/ml, Preprotech). For immunofluorescence analyses, 4×10^4 epicardial cells were cultured into 24-well plates containing gelatin-coated glass coverslips for 18 h, followed by treatment with or without BMP4 (100 ng/ml) for 48 h.

Western blot analysis of immortalised epicardial cells

For western blot analyses, treated immortalised epicardial cells were lysed using SDS buffer (1.5 M Tris pH 6.8, 15% glycerol, 3% SDS, 7.5% β-mercaptoethanol and 0.0375% Bromophenol Blue). Lysates were separated by SDS-PAGE gel and transferred to PVDF membranes for immunoblotting. Immunoblots were incubated overnight at 4°C with antibodies against p-Smad1/5 (1:1000; Cell Signaling), Smad1/5/8 (1:1000; Santa Cruz Biotechnology) see Table S7.

Immunofluorescence

Confluent epicardial cell monolayers grown on gelatin-coated glass coverslips were washed with PBS and fixed at room temperature with 4% PFA in PBS for 12 min and then permeabilised using 0.1% Triton X-100 in PBS for 7 min. After permeabilisation, cells were washed with PBS and blocked with PBS containing 1% bovine serum albumin (BSA) for 30 min at room temperature. Fixed cells were stained overnight at 4°C with an antibody against β-catenin (1:250, BD Transduction Laboratories); see Table S6. After washing with PBS three times, fixed cells were labelled with an Alexa Fluor 546 anti-mouse IgG (Molecular Probes, A11003) for 1 h in the dark at room temperature. After staining, the coverslips were mounted in Fluoromount (Sigma-Aldrich). The images were acquired using a Leica TCS SP5 confocal laser scanning microscope (Leica Microsystems) equipped with a DMI6000 inverted microscope, and Argon (458/476/488/514), diode-pumped solid-state (561 nm) and HeNe (633) lasers. The Alexa

488 and Alexa 546 images were acquired sequentially using 488 and 561 laser lines, an acoustic optical beam splitter (AOBS) and emission detection ranges of 500–555 and 571–625, respectively. Confocal *z*-stack *xy* plane images were taken at 0.21 μm intervals at a total depth of 7 μm . The *xy* or *xz* section images were generated from *z*-stack images with Leica software. Images for direct comparison were obtained under identical parameters and were representative of three different assays. The final analysis of all images was performed using ImageJ software. Cell height was measured by reconstructing the monolayer as a *z*-stack and drawing a line from the basal border of the monolayer to the bottom of the coverslip. Cell area was measured in *xy* sections by drawing a line around the circumference of each cell at its midsection.

FACS analysis

Embryonic mouse heart ventricles and lungs from *Wt1^{GFP}* mice at different stages of development were dissected and dissociated into single cells using a solution containing trypsin solution diluted 1:10 [stock solution: 0.2% trypsin (Sigma-Aldrich, T4799) in PBS, pH 7.8], 0.13 mM EDTA (Fisher Scientific, D/0700/53) and 0.003% Phenol Red solution (Sigma-Aldrich, P0290) diluted in PBS, using a heated shaking block (Eppendorf Thermomixer compact) at 37°C and 1000 rpm. Dissociated cells were placed every 10 min into a 1.5 ml tube containing DMEM (Gibco) medium with 10% BSA, and kept on ice. The dissociating solution was replaced and the process repeated until most of the heart was dissociated. FACS sorting of GFP populations was carried out by gating against a GFP-negative control littermate. The proportion of dead cells was assessed using 50 $\mu\text{g}/\text{ml}$ propidium iodide. Cells were sorted on a BD Bioscience FACSARIA II and data were analysed using BD FACSDiva software (v6.1.3).

In situ hybridisation

Mouse heart cryosections with a thickness of 12 μm were used for mRNA *in situ* hybridisations and stored at -80°C . To make digoxigenin (DIG)-labelled probes, the primers listed in Table S8 were used to amplify a region of the coding sequence for each gene indicated, where the reverse primer is linked to a T7 polymerase promoter tag sequence.

The PCR product was electrophoresed on a 1% agarose gel, and an appropriately sized band was cut out and purified (QIAquick Gel Extraction Kit, 28706) for use as a template in a second round of PCR, agarose gel electrophoresis and purification. Following sequence verification, 200 ng of each PCR product was used for the production of DIG-labelled riboprobes (Roche DIG RNA Labelling Kit SP6/T7, 11175025910) as per the manufacturer's instructions, and re-suspended in RNase-free water. *In situ* hybridisations were performed with modifications, as described previously (Kurrasch et al., 2007), with sections from three embryos hybridised to each probe and probes that detected consistent patterns of expression used.

RNAscope for *Bmp4* was performed on a Leica Biosystems BOND RX research staining robot (Leica Biosystems), as follows: frozen sections were removed from storage at -80°C and fixed immediately in pre-cooled ice cold 4% neutral buffered formaldehyde, followed by 5 min incubations at room temperature in 50%, 70% and 100% ethanol. Slides were then placed onto an RX staining robot and stained using the ACD Bio LS 2.5 Brown RNAscope assay (ACD, 401308), as per the manufacturer's recommendations. Appropriate control probes (PPIB and DapB) were used to determine that the optimal pre-treatment conditions were 20 min incubation with protease only. The *Bmp4* probe was stained under identical conditions. RNAscope staining slides were then counterstained with Haematoxylin, dehydrated in graded ethanol, cleared in xylene and coverslipped with Pertex.

Chromatin IP

Immortalised epicardial cells were dissociated with 1:10 diluted trypsin and fixed with 1% formaldehyde (Calbiochem, 344198). Crosslinking was stopped by adding 0.125 M glycine. Chromatin immunoprecipitation was carried out as previously described (Velecela et al., 2013), with the following modifications: magnetic Dynabeads Protein A (Thermo Fisher Scientific, 1001D) were used for immunoprecipitations with antibodies against WT1 (Abcam, ab89901) and rabbit IgG (Sigma-Aldrich, I8140) as a control. Eluted DNA was quantified by qPCR using SYBR Select Master

Mix (Life Technologies, 4472920), with the primers and annealing temperatures indicated in Table S9.

Isolation and amplification of RNA for microarray analysis

The two populations of *Wt1-GFP*-positive cells, *Wt1GFP^{+/+}* and *Wt1GFP⁺*, were isolated by FACS from *Wt1^{GFP}* heart ventricles at different stages of development and collected in DMEM medium (Thermo Fisher Scientific, 10569010) with 10% fetal calf serum, pelleted by gentle centrifugation and RNA extracted using a PicoPure RNA Isolation Kit (Thermo Fisher Scientific, KIT0204), according to the manufacturer's instructions, then stored at -80°C .

RNA from at least ten embryonic hearts was pooled by embryonic stage to make one replicate. Three replicates per stage were used for the analysis. RNA quality was assessed using the Agilent 2100 Bioanalyzer platform. The Illumina TotalPrep RNA Amplification Kit (Thermo Fisher Scientific, AMIL1791) was used to generate biotinylated amplified RNA, with 100 ng of total RNA per replicate.

RNA was also isolated from *Wt1GFP^{+/+}* FACS-sorted cells from control and *epiWt1KO* heart ventricles at E13.5. The RiboAmp HS PLUS Kit (Thermo Fisher Scientific, KIT0525) was used to amplify 5 ng of total RNA per replicate, followed by Biotin Turbo Labelling (Thermo Fisher Scientific, KIT0608), as per the manufacturer's instructions.

Microarray analysis

MouseWG-6 V2 BeadChips from Illumina were used for gene expression profiling. All samples were analysed in biological triplicates. Samples were quantiles normalised in R; statistical differences were assessed by ANOVA, with the false discovery rate based on permutations $P < 0.05$. Transcripts regulated more than twice in at least one condition were considered significantly regulated. For principal components analysis and hierarchical clustering, we used ClustVis (PMID: 25969447). Interactome analysis was performed on STRINGdb.

Real-time PCR of in vivo samples

Amplified RNA without the addition of biotin from *Wt1GFP* FACS-sorted cells was used for reverse transcription and cDNA generation with SuperScript III Reverse Transcriptase (Thermo Fisher Scientific, 18080044). Relative expression levels were determined with SYBR Select Master Mix (Thermo Fisher Scientific, 4472897). Real-time PCR experiments were performed on a LightCycler 480 System (Roche). Error bars indicate the standard error for three biological replicates. The primers used are listed in Table S10.

Ex vivo and in vivo BMP4 signalling inhibition experiments

For *ex vivo* rescue experiments, briefly, a solution of 1% agarose (Sigma-Aldrich) was dispensed into a 24-well plate and allowed to solidify in the hood, and the agarose excess was then removed. Agarose gels were washed several times with DMEM. Control and *epiWt1KO* E13.5 heart ventricles were cultured in the agarose-coated 24-well plate containing medium with dorsomorphin (4 μM , Sigma-Aldrich) or DMSO as vehicle controls. The hearts were incubated at 37°C for 48 h.

For *ex vivo* LDN-treated heart experiments, E11.5 heart ventricles from *Wt1^{GFP}* mice were cultured in 1% agarose-coated well plates containing medium with LDN-193189, or endotoxin-free water as vehicle controls. The hearts were incubated at 37°C overnight. RNA from *Wt1GFP^{+/+}* FACS-sorted cells was obtained with a Total RNA Purification Kit (Norgen, 17200). RNA was then used for reverse transcription and amplification with a QuantiTect Whole Transcriptome Kit (Qiagen). Real-time PCR experiments were performed as above.

For *in vivo* rescue experiments, *Gata5Cre⁺; Wt1^{gfp/+}* males and *Wt1^{loxP/loxP}* female mice were set up for timed matings as described above, and pregnant females were treated with the BMP inhibitor LDN-193189 via intraperitoneal injections from E13.5. LDN-193189 was dissolved in endotoxin-free water (Sigma-Aldrich, 95289) at 1.5 mg/ml and neutralised at pH 6.8. The dosage per injection was 6 mg/kg, twice per day. Control females received an equivalent volume of endotoxin-free water via intraperitoneal injections. Embryos were collected at E15.5 and fixed for TEM or immunostaining analysis, as described above.

For *in vivo* LDN-193189 treatment of the early epicardium, pregnant CD1 female mice were given LDN-193189 or endotoxin-free water as a control via intraperitoneal injections twice per day from E9.5, using the same dosage and concentration as above, up to and including day E12.5. Embryos were collected at E12.5, fixed and embedded in paraffin for immunostaining analysis, as above.

Biotin epicardial permeability assay

An EZ-Link Sulfo-NHS-LC-Biotin (Thermo Fisher Scientific) solution was freshly prepared and diluted at a concentration of 1 mg/ml in PBS. Mouse embryos were dissected and placed in PBS. An opening in the chest pericardial cavity was made using forceps, and 10 μ l of biotin was pipetted into the opening and allowed to perfuse for 5 min. Biotin was subsequently quenched with 100 mM glycine in PBS solution to remove excess biotin. Embryos were then fixed in 4% PFA overnight, paraffin-embedded and sectioned. The sections were subsequently deparaffinised, then subjected to heat-induced antigen retrieval and blocked in 10% goat serum. The sections were incubated with Rhodamine Red-X-conjugated streptavidin (Invitrogen) for 30 min at room temperature, as per the manufacturer's instructions, to detect biotin prior to imaging using a Nikon confocal microscope system A1+.

Lung RT-qPCR

RNA from lung *Wt1*GFP+ FACS-sorted cells was obtained with a Total RNA Purification Kit (Norgen, 17200). RNA was then used for reverse transcription and amplification with a QuantiTect Whole Transcriptome Kit (Qiagen). Real-time PCR experiments were performed as above.

Quantification and statistical analysis

Data are presented as mean \pm s.e.m. Statistical significance between two groups was determined by unpaired, two-tailed Student's *t*-tests. We applied nonparametric one-way ANOVA followed by Tukey's post-hoc test to evaluate the differences among multiple groups of samples.

Acknowledgements

We thank Elisabeth Freyer for her assistance and for running the FACS facility (MRC HGU, IGMM, Edinburgh, UK), Craig Nicol for his assistance with Fig. 8 (MRC HGU, IGMM, Edinburgh, UK) and Robert Hill and Ian Adams (MRC HGU, IGMM, Edinburgh, UK) for critical reading of the manuscript.

Competing interests

The authors declare no competing or financial interests.

Author contributions

Conceptualization: O.M.M.-E.; Methodology: V.V., Y.-Y.C.; Formal analysis: V.V., A.T.-C., A.G.-M., M.R.-P., C.M.-S., M.S.-M., B.C.-B., M.R., F.X.S., F.O.M., O.M.M.-E.; Investigation: V.V., A.T.-C., A.G.-M., M.R.-P., C.M.-S., Y.-Y.C.; Resources: N.D.H.; Data curation: F.O.M.; Writing - original draft: O.M.M.-E.; Writing - review & editing: V.V., O.M.M.-E.; Supervision: O.M.M.-E.; Funding acquisition: N.D.H., F.X.S., O.M.M.-E.

Funding

This work was supported by the Fundació La Marató de TV3 (20152210 to O.M.M.-E.), the Ministerio de Economía y Competitividad/European Regional Development Fund (BFU2015-68135-P to O.M.M.-E., SAF2017-86622-C2-1-R to F.X.S.), a British Heart Foundation grant (PG/15/29/31388 to N.D.H.) and a core grant from the Medical Research Council (to N.D.H.). V.V. was supported by a Daniel Bravo Andreu Foundation (Fundació Privada Daniel Bravo Andreu) fellowship.

Data availability

Microarray data have been deposited in the NCBI Gene Expression Omnibus database under accession number GSE113276.

Supplementary information

Supplementary information available online at <http://dev.biologists.org/lookup/doi/10.1242/dev.178723.supplemental>

References

Baek, S. T. and Tallquist, M. D. (2012). Nf1 limits epicardial derivative expansion by regulating epithelial to mesenchymal transition and proliferation. *Development* **139**, 2040-2049. doi:10.1242/dev.074054

- Bianchi, A., Gervasi, M. E. and Bakin, A. (2010). Role of beta5-integrin in epithelial-mesenchymal transition in response to TGF-beta. *Cell Cycle* **9**, 1647-1659. doi:10.4161/cc.9.8.11517
- Bochmann, L., Sarathchandra, P., Mori, F., Lara-Pezzi, E., Lazzaro, D. and Rosenthal, N. (2010). Revealing new mouse epicardial cell markers through transcriptomics. *PLoS ONE* **5**, e11429. doi:10.1371/journal.pone.0011429
- Byrnes, L. E., Wong, D. M., Subramaniam, M., Meyer, N. P., Gilchrist, C. L., Knox, S. M., Tward, A. D., Ye, C. J. and Sneddon, J. B. (2018). Lineage dynamics of murine pancreatic development at single-cell resolution. *Nat. Commun.* **9**, 3922. doi:10.1038/s41467-018-06176-3
- Cano, E., Carmona, R., Ruiz-Villalba, A., Rojas, A., Chau, Y.-Y., Wagner, K. D., Wagner, N., Hastie, N. D., Muñoz-Chápuli, R. and Pérez-Pomares, J. M. (2016). Extracardiac septum transversum/proepicardial endothelial cells pattern embryonic coronary arterio-venous connections. *Proc. Natl. Acad. Sci. USA* **113**, 656-661. doi:10.1073/pnas.1509834113
- Cao, J., Navis, A., Cox, B. D., Dickson, A. L., Gemberling, M., Karra, R., Bagnat, M. and Poss, K. D. (2016). Single epicardial cell transcriptome sequencing identifies Caveolin 1 as an essential factor in zebrafish heart regeneration. *Development* **143**, 232-243. doi:10.1242/dev.130534
- Chau, Y. Y., Brownstein, D., Mjoseng, H., Lee, W.-C., Buza-Vidas, N., Nerlov, C., Jacobsen, S. E., Perry, P., Berry, R., Thornburn, A. et al. (2011). Acute multiple organ failure in adult mice deleted for the developmental regulator Wt1. *PLoS Genet.* **7**, e1002404. doi:10.1371/journal.pgen.1002404
- Combs, M. D., Braitsch, C. M., Lange, A. W., James, J. F. and Yutzey, K. E. (2011). NFATC1 promotes epicardium-derived cell invasion into myocardium. *Development* **138**, 1747-1757. doi:10.1242/dev.060996
- del Monte, G., Casanova, J. C., Guadix, J. A., MacGrogan, D., Burch, J. B. E., Pérez-Pomares, J. M. and de la Pompa, J. L. (2011). Differential Notch signaling in the epicardium is required for cardiac inflow development and coronary vessel morphogenesis. *Circ. Res.* **108**, 824-836. doi:10.1161/CIRCRESAHA.110.229062
- Dube, K. N., Thomas, T. M., Munshaw, S., Rohling, M., Riley, P. R. and Smart, N. (2017). Recapitulation of developmental mechanisms to revascularize the ischemic heart. *JCI insight* **2**, 96800. doi:10.1172/jci.insight.96800
- Firth, S. M. and Baxter, R. C. (2002). Cellular actions of the insulin-like growth factor binding proteins. *Endocr. Rev.* **23**, 824-854. doi:10.1210/er.2001-0033
- Genander, M., Cook, P. J., Ramsköld, D., Keyes, B. E., Mertz, A. F., Sandberg, R. and Fuchs, E. (2014). BMP signaling and its pSMAD1/5 target genes differentially regulate hair follicle stem cell lineages. *Cell Stem Cell* **15**, 619-633. doi:10.1016/j.stem.2014.09.009
- Gomez, J. M., Wang, Y. and Riechmann, V. (2012). Tao controls epithelial morphogenesis by promoting Fasciclin 2 endocytosis. *J. Cell Biol.* **199**, 1131-1143. doi:10.1083/jcb.201207150
- Guadix, J. A., Ruiz-Villalba, A., Lettice, L., Velecela, V., Munoz-Chapuli, R., Hastie, N. D., Perez-Pomares, J. M. and Martínez-Estrada, O. M. (2011). Wt1 controls retinoic acid signalling in embryonic epicardium through transcriptional activation of Raldh2. *Development* **138**, 1093-1097. doi:10.1242/dev.044594
- Hartwig, S., Ho, J., Pandey, P., Macisaac, K., Taglienti, M., Xiang, M., Alterovitz, G., Ramoni, M., Fraenkel, E. and Kreidberg, J. A. (2010). Genomic characterization of Wilms' tumor suppressor 1 targets in nephron progenitor cells during kidney development. *Development* **137**, 1189-1203. doi:10.1242/dev.045732
- Hastie, N. D. (2017). Wilms' tumour 1 (WT1) in development, homeostasis and disease. *Development* **144**, 2862-2872. doi:10.1242/dev.153163
- Hosen, N., Shirakata, T., Nishida, S., Yanagihara, M., Tsuboi, A., Kawakami, M., Oji, Y., Oka, Y., Okabe, M., Tan, B. et al. (2007). The Wilms' tumor gene WT1-GFP knock-in mouse reveals the dynamic regulation of WT1 expression in normal and leukemic hematopoiesis. *Leukemia* **21**, 1783-1791. doi:10.1038/sj.leu.2404752
- Ishii, Y., Garriock, R. J., Navetta, A. M., Coughlin, L. E. and Mikawa, T. (2010). BMP signals promote proepicardial protrusion necessary for recruitment of coronary vessel and epicardial progenitors to the heart. *Dev. Cell* **19**, 307-316. doi:10.1016/j.devcel.2010.07.017
- Komiyama, M., Ito, K. and Shimada, Y. (1987). Origin and development of the epicardium in the mouse embryo. *Anat. Embryol. (Berl)* **176**, 183-189. doi:10.1007/BF00310051
- Kruithof, B. P., van Wijk, B., Somi, S., Kruithof-de Julio, M., Pérez Pomares, J. M., Weesie, F., Wessels, A., Moorman, A. F. and van den Hoff, M. J. (2006). BMP and FGF regulate the differentiation of multipotential pericardial mesoderm into the myocardial or epicardial lineage. *Dev. Biol.* **295**, 507-522. doi:10.1016/j.ydbio.2006.03.033
- Kurrasch, D. M., Cheung, C. C., Lee, F. Y., Tran, P. V., Hata, K. and Ingraham, H. A. (2007). The neonatal ventromedial hypothalamus transcriptome reveals novel markers with spatially distinct patterning. *J. Neurosci.* **27**, 13624-13634. doi:10.1523/JNEUROSCI.2858-07.2007
- Lehembre, F., Yilmaz, M., Wicki, A., Schomber, T., Strittmatter, K., Ziegler, D., Kren, A., Went, P., Derksen, P. W., Berns, A. et al. (2008). NCAM-induced focal adhesion assembly: a functional switch upon loss of E-cadherin. *EMBO J.* **27**, 2603-2615. doi:10.1038/emboj.2008.178

- Lepilina, A., Coon, A. N., Kikuchi, K., Holdway, J. E., Roberts, R. W., Burns, C. G. and Poss, K. D. (2006). A dynamic epicardial injury response supports progenitor cell activity during zebrafish heart regeneration. *Cell* **127**, 607-619. doi:10.1016/j.cell.2006.08.052
- Liu, J. and Stainier, D. Y. R. (2010). Tbx5 and Bmp signaling are essential for proepicardium specification in zebrafish. *Circ. Res.* **106**, 1818-1828. doi:10.1161/CIRCRESAHA.110.217950
- Lockhart, M. M., Boukens, B. J., Phelps, A. L., Brown, C.-L. M., Toomer, K. A., Burns, T. A., Mukherjee, R. D., Norris, R. A., Trusk, T. C., van den Hoff, M. J. B. et al. (2014). Alk3 mediated Bmp signaling controls the contribution of epicardially derived cells to the tissues of the atrioventricular junction. *Dev. Biol.* **396**, 8-18. doi:10.1016/j.ydbio.2014.09.031
- Martínez-Estrada, O. M., Lettice, L. A., Essafi, A., Guadix, J. A., Slight, J., Vevelcel, V., Hall, E., Reichmann, J., Devenney, P. S., Hohenstein, P. et al. (2010). Wt1 is required for cardiovascular progenitor cell formation through transcriptional control of Snail and E-cadherin. *Nat. Genet.* **42**, 89-93. doi:10.1038/ng.494
- Massaia, A., Chaves, P., Samari, S., Miragaia, R. J., Meyer, K., Teichmann, S. A. and Nosedá, M. (2018). Single cell gene expression to understand the dynamic architecture of the heart. *Front. Cardiovasc Med.* **5**, 167. doi:10.3389/fcvm.2018.00167
- McClure, K. D. and Schubiger, G. (2005). Developmental analysis and squamous morphogenesis of the peripodial epithelium in *Drosophila* imaginal discs. *Development* **132**, 5033-5042. doi:10.1242/dev.02092
- Miquero, L. and Kelly, R. G. (2013). Organogenesis of the vertebrate heart. *Wiley Interdiscip. Rev. Dev. Biol.* **2**, 17-29. doi:10.1002/wdev.68
- Moore, A. W., McInnes, L., Kreidberg, J., Hastie, N. D. and Schedl, A. (1999). YAC complementation shows a requirement for Wt1 in the development of epicardium, adrenal gland and throughout nephrogenesis. *Development* **126**, 1845-1857.
- Motamedji, F. J., Badro, D. A., Clarkson, M., Rita Lecca, M., Bradford, S. T., Buske, F. A., Saar, K., Hubner, N., Brandli, A. W. and Schedl, A. (2014). WT1 controls antagonistic FGF and BMP-pSMAD pathways in early renal progenitors. *Nat. Commun.* **5**, 4444. doi:10.1038/ncomms5444
- Nilsson, E. E. and Skinner, M. K. (2003). Bone morphogenetic protein-4 acts as an ovarian follicle survival factor and promotes primordial follicle development. *Biol. Reprod.* **69**, 1265-1272. doi:10.1095/biolreprod.103.018671
- Perez-Pomares, J. M. and de la Pompa, J. L. (2011). Signaling during epicardium and coronary vessel development. *Circ. Res.* **109**, 1429-1442. doi:10.1161/CIRCRESAHA.111.245589
- Porrello, E. R., Mahmoud, A. I., Simpson, E., Hill, J. A., Richardson, J. A., Olson, E. N. and Sadek, H. A. (2011). Transient regenerative potential of the neonatal mouse heart. *Science* **331**, 1078-1080. doi:10.1126/science.1200708
- Schlueter, J., Männer, J. and Brand, T. (2006). BMP is an important regulator of proepicardial identity in the chick embryo. *Dev. Biol.* **295**, 546-558. doi:10.1016/j.ydbio.2006.03.036
- Sharma, B., Chang, A. and Red-Horse, K. (2017). Coronary artery development: progenitor cells and differentiation pathways. *Annu. Rev. Physiol.* **79**, 1-19. doi:10.1146/annurev-physiol-022516-033953
- Simoës, F. C. and Riley, P. R. (2018). The ontogeny, activation and function of the epicardium during heart development and regeneration. *Development* **145**, dev155994. doi:10.1242/dev.155994
- Singh, A., Ramesh, S., Cibi, D. M., Yun, L. S., Li, J., Li, L., Manderfield, L. J., Olson, E. N., Epstein, J. A. and Singh, M. K. (2016). Hippo signaling mediators Yap and Taz are required in the epicardium for coronary vasculature development. *Cell Reports* **15**, 1384-1393. doi:10.1016/j.celrep.2016.04.027
- Smart, N., Bollini, S., Dube, K. N., Vieira, J. M., Zhou, B., Davidson, S., Yellon, D., Riegler, J., Price, A. N., Lythgoe, M. F. et al. (2011). De novo cardiomyocytes from within the activated adult heart after injury. *Nature* **474**, 640-644. doi:10.1038/nature10188
- Tran, J. R., Zheng, X. and Zheng, Y. (2016). Lamin-B1 contributes to the proper timing of epicardial cell migration and function during embryonic heart development. *Mol. Biol. Cell* **27**, 3956-3963. doi:10.1091/mbc.e16-06-0462
- Trescos, Y., Tessier, E., Rougeaux, C., Goossens, P. L. and Tournier, J.-N. (2015). Micropatterned macrophage analysis reveals global cytoskeleton constraints induced by *Bacillus anthracis* edema toxin. *Infect. Immun.* **83**, 3114-3125. doi:10.1128/IAI.00479-15
- van Wijk, B., Gunst, Q. D., Moorman, A. F. M. and van den Hoff, M. J. B. (2012). Cardiac regeneration from activated epicardium. *PLoS ONE* **7**, e44692. doi:10.1371/journal.pone.0044692
- Vevelcel, V., Lettice, L. A., Chau, Y.-Y., Slight, J., Berry, R. L., Thornburn, A., Gunst, Q. D., van den Hoff, M., Reina, M., Martinez, F. O. et al. (2013). WT1 regulates the expression of inhibitory chemokines during heart development. *Hum. Mol. Genet.* **22**, 5083-5095. doi:10.1093/hmg/ddt358
- Wang, P.-C., Weng, C.-C., Hou, Y.-S., Jian, S.-F., Fang, K.-T., Hou, M.-F. and Cheng, K.-H. (2014a). Activation of VCAM-1 and its associated molecule CD44 leads to increased malignant potential of breast cancer cells. *Int. J. Mol. Sci.* **15**, 3560-3579. doi:10.3390/ijms15033560
- Wang, R. N., Green, J., Wang, Z., Deng, Y., Qiao, M., Peabody, M., Zhang, Q., Ye, J., Yan, Z., Denduluri, S. et al. (2014b). Bone morphogenetic protein (BMP) signaling in development and human diseases. *Genes Dis.* **1**, 87-105. doi:10.1016/j.gendis.2014.07.005
- Wu, M., Smith, C. L., Hall, J. A., Lee, I., Luby-Phelps, K. and Tallquist, M. D. (2010). Epicardial spindle orientation controls cell entry into the myocardium. *Dev. Cell* **19**, 114-125. doi:10.1016/j.devcel.2010.06.011
- Xiao, Y., Hill, M. C., Zhang, M., Martin, T. J., Morikawa, Y., Wang, S., Moise, A. R., Wythe, J. D. and Martin, J. F. (2018). Hippo signaling plays an essential role in cell state transitions during cardiac fibroblast development. *Dev. Cell* **45**, 153-169.e156. doi:10.1016/j.devcel.2018.03.019
- Yu, P. B., Deng, D. Y., Lai, C. S., Hong, C. C., Cuny, G. D., Bouxsein, M. L., Hong, D. W., McManus, P. M., Katagiri, T., Sachidanandan, C. et al. (2008). BMP type I receptor inhibition reduces heterotopic [corrected] ossification. *Nat. Med.* **14**, 1363-1369. doi:10.1038/nm.1888
- Zamora, M., Manner, J. and Ruiz-Lozano, P. (2007). Epicardium-derived progenitor cells require beta-catenin for coronary artery formation. *Proc. Natl. Acad. Sci. USA* **104**, 18109-18114. doi:10.1073/pnas.0702415104
- Zhao, G.-Q. (2003). Consequences of knocking out BMP signaling in the mouse. *Genesis* **35**, 43-56. doi:10.1002/gene.10167
- Zhou, B., Ma, Q., Rajagopal, S., Wu, S. M., Domian, I., Rivera-Feliciano, J., Jiang, D., von Gise, A., Ikeda, S., Chien, K. R. et al. (2008). Epicardial progenitors contribute to the cardiomyocyte lineage in the developing heart. *Nature* **454**, 109-113. doi:10.1038/nature07060
- Zhou, B., Honor, L. B., He, H., Ma, Q., Oh, J.-H., Butterfield, C., Lin, R.-Z., Melero-Martin, J. M., Dolmatova, E., Duffy, H. S. et al. (2011). Adult mouse epicardium modulates myocardial injury by secreting paracrine factors. *J. Clin. Invest.* **121**, 1894-1904. doi:10.1172/JCI45529

Fig. S1

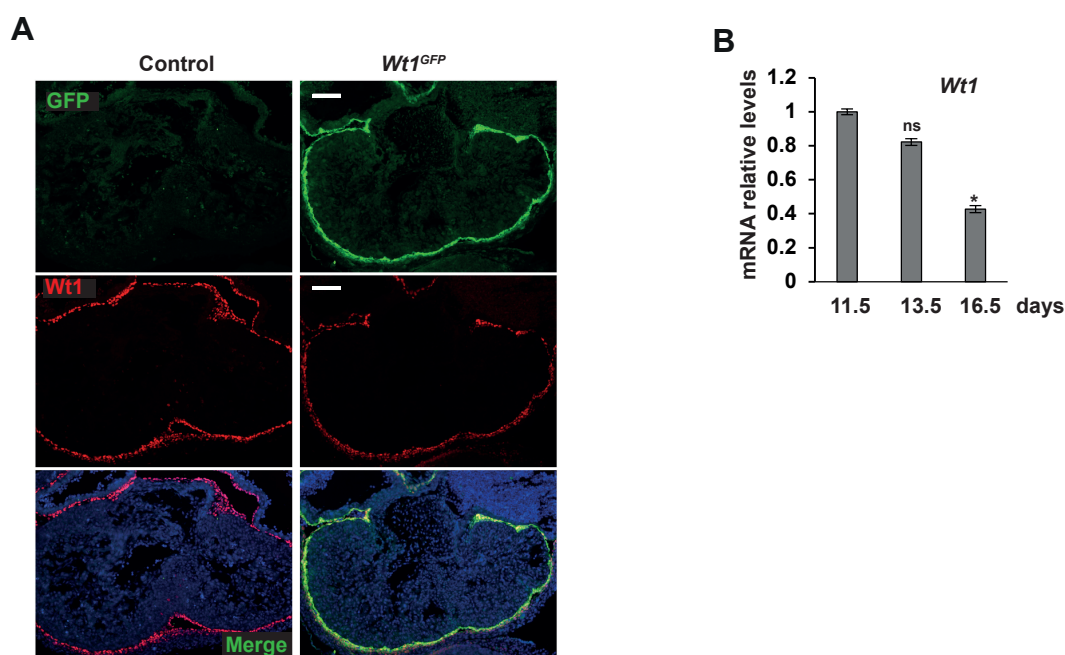


Figure S1. Immunofluorescence analyses of Wt1 and GFP in heart sections of *Wt1^{GFP}* mice. (A) Immunofluorescent staining for GFP (green) and Wt1 (red) and nuclear Hoechst stain (blue) using sections from E11.5 wild type littermates and *Wt1^{GFP}* embryonic hearts, where the double staining for Wt1 and GFP can clearly be seen in the epicardium. (B) qRT-PCR analysis of *Wt1* in *Wt1^{GFP}⁺⁺* FACS-sorted epicardial enriched cells from *Wt1^{GFP}* mice at different days of development. Error bars represent \pm s.e.m. and p-values are based on $*P < 0.05$, one-way ANOVA followed by Tukey's post hoc test. RNA from FACS-isolated cells from at least 10 embryonic hearts was pooled by embryonic stage. Three replicates per condition were used for the analysis. Scale bars, 100 μ m.

Fig. S2

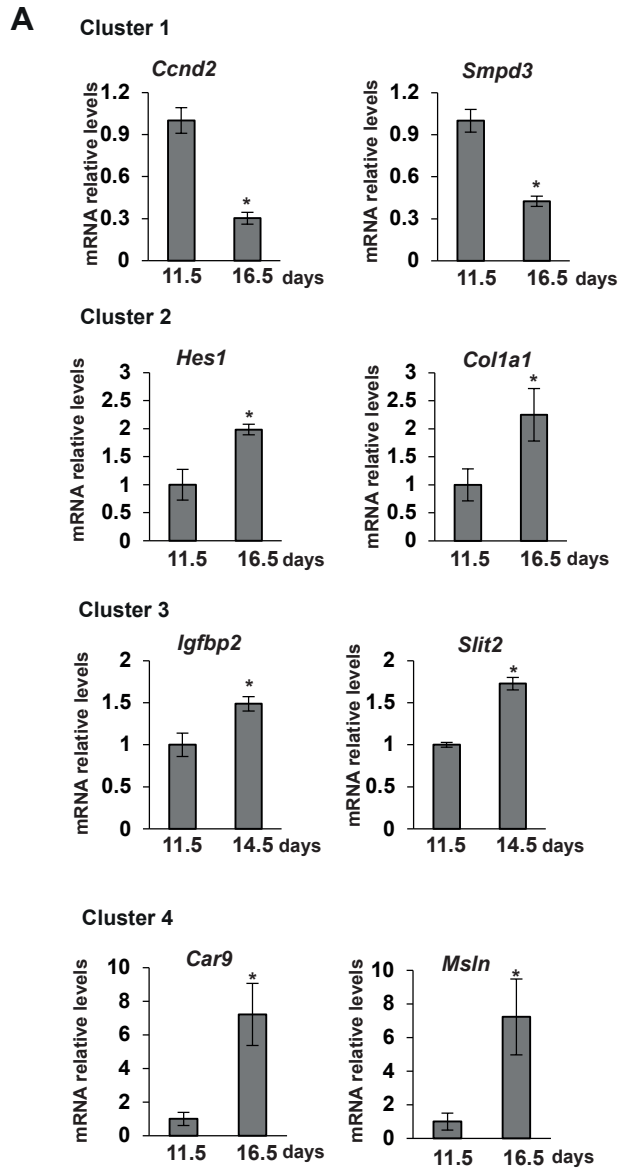


Fig. S2 B

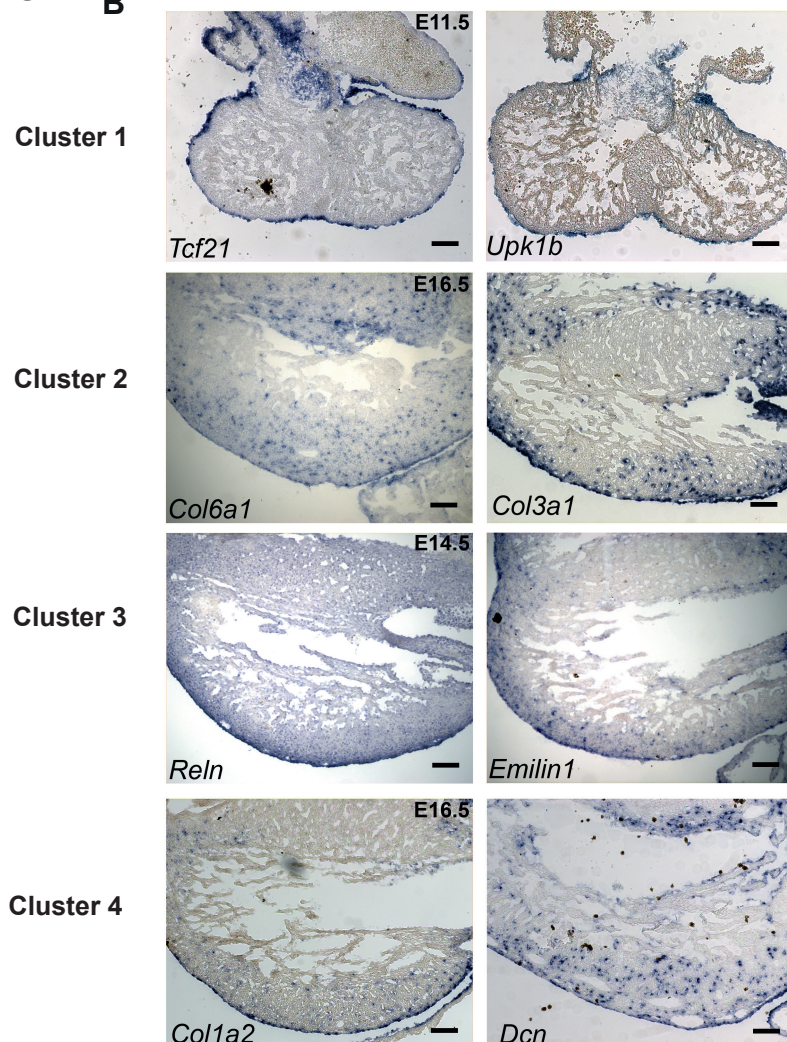


Figure S2. Validation of genes included in different clusters. (A) qRT-PCR analysis of indicated genes in *Wt1*^{GFP}⁺ FACS-sorted epicardial enriched cells from *Wt1*^{GFP} mice at different days of development. Two genes per cluster are shown in each panel. Error bars represent \pm s.e.m. and p-values are based on $*P < 0.05$, two-tailed *t*-tests. RNA from FACS-isolated cells from at least 10 embryonic hearts was pooled by embryonic stage. Three replicates per condition were used for the analysis. (B) *In situ* mRNA hybridisation analyses of indicated genes in embryonic heart sections. Two genes from each cluster were analysed and their expression was found to be highly enriched in the embryonic epicardium. Scale bars, 100 μ m.

Fig. S3

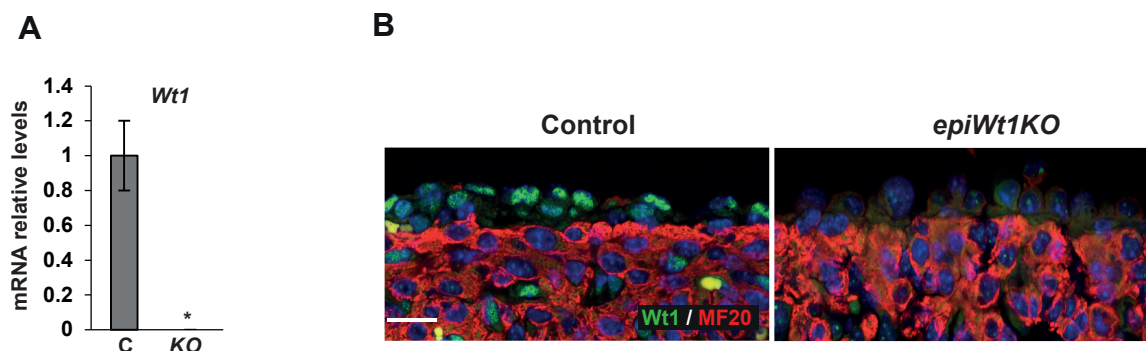


Figure S3. Efficient deletion of *Wt1* in the epicardium of *epiWt1KO* mouse model. (A) qRT-PCR analysis of *Wt1* expression in *Wt1GFP⁺⁺* FACS-sorted epicardial cells from control and *epiWt1KO* ventricles at E13.5. Error bars represent \pm s.e.m. and p-values are based on $*P < 0.05$, two-tailed *t*-tests. RNA from FACS-isolated cells from at least 10 embryonic hearts was pooled to make one replicate. Three replicates per condition were used for the analysis. (B) Immunofluorescent staining for *Wt1* (green), the cardiac myosin marker MF20 (red) and nuclear Hoechst stain (blue), in heart sections from a littermate control and *epiWt1KO* hearts at stage E15.5. Scale bar, 20 μ m.

Fig. S4

A

Gene symbol	KO vs Control
<i>Figf</i>	13.13 ± 3.54*
<i>Car9</i>	9.37 ± 0.85*
<i>Thy1</i>	6.15 ± 2.02*
<i>Cdkn2b</i>	5.43 ± 1.63*
<i>Krt17</i>	3.88 ± 1.59*
<i>Smpd3</i>	3.65 ± 0.43*
<i>Egfr</i>	3.58 ± 1.08*
<i>Slc9a3r1</i>	2.72 ± 0.71*
<i>Krt14</i>	2.41 ± 0.74*
<i>Bmp4</i>	2.39 ± 0.11*
<i>Fah</i>	2.23 ± 0.80
<i>Col1a1</i>	2.21 ± 0.22*
<i>Cldn15</i>	2.21 ± 0.55*
<i>Krt7</i>	2.05 ± 0.29*
<i>Col1a2</i>	1.20 ± 0.30
<i>Col12a1</i>	1.19 ± 0.79
<i>Slit2</i>	0.31 ± 0.08*
<i>Nbl1</i>	0.31 ± 0.28*

B

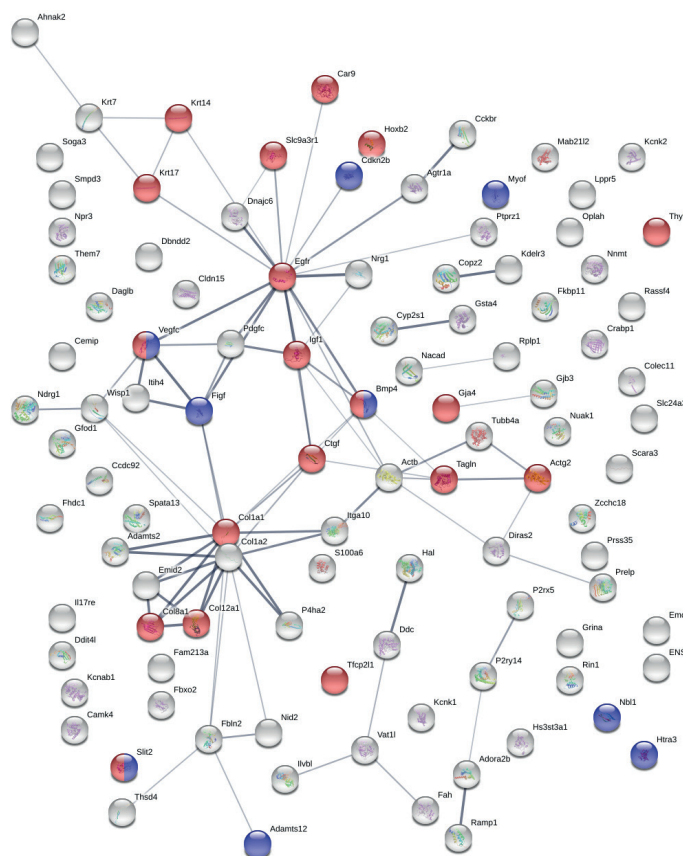


Figure S4. Validation of genes differentially expressed in *Wt1GFP⁺⁺* epicardial-enriched cells from control and *epiWt1KO*. (A) qRT-PCR analysis of indicated genes from our microarray analysis of *Wt1GFP⁺⁺* epicardial cells from control and *epiWt1KO* mice at E13.5. Values are expressed as fold change over control. P-values are based on two-tailed *t*-tests, *P<0.05. RNA from FACS-isolated cells from at least 10 embryonic hearts was pooled by condition. Three replicates per condition were used for the analysis. (B) STRINGdb interactome of regulated genes, indicating genes involved in the categories of tissue morphogenesis (red) and regulation of cellular response to growth factor stimulus (blue).

Fig. S5

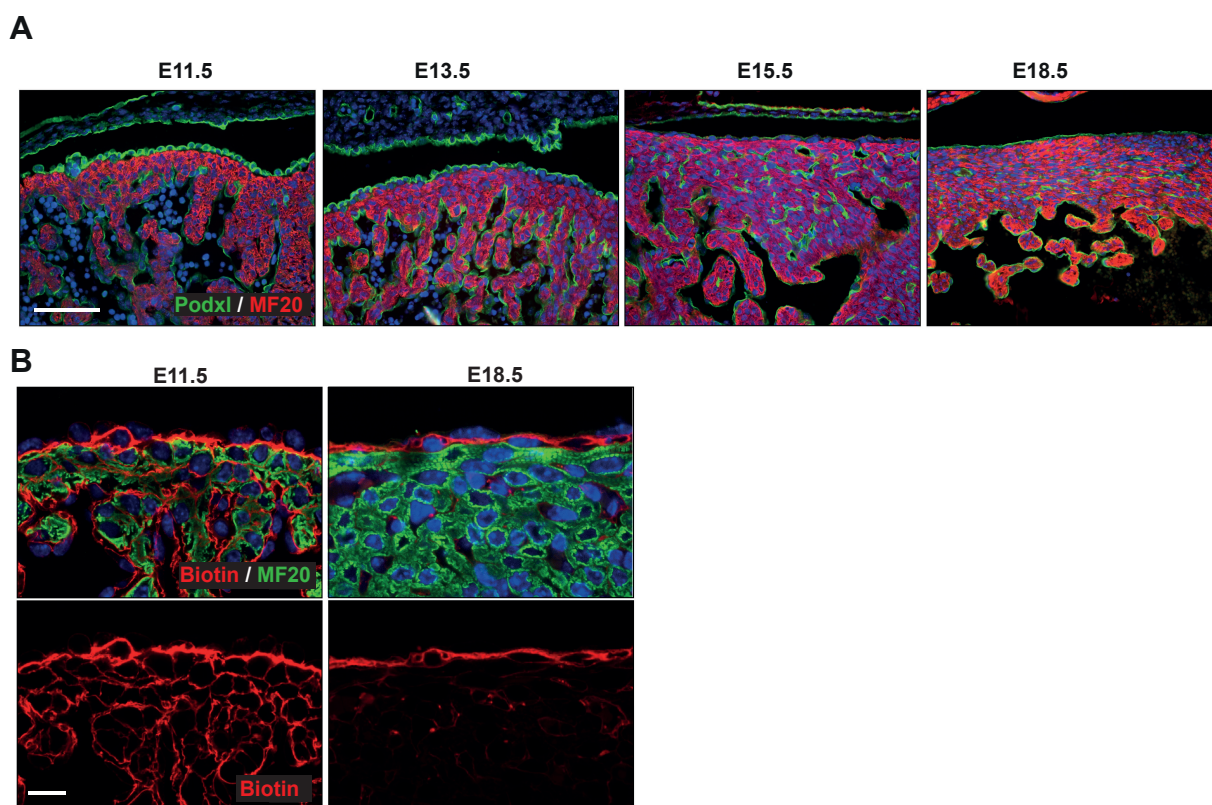


Figure S5. The mature epicardium displays a squamous non-permeable phenotype. (A) Representative low magnification images of the immunofluorescent staining for podocalyxin in green, MF20 (red) and nuclear Hoechst stain (blue), using heart sections at different days of development, from E11.5 to E18.5. Sections of ventricles indicate the epicardial transition from a cuboidal cell shape in the early stages to a flattened shape later on. (B) Biotin permeability assay of the E11.5 and E18.5 epicardium. Biotin was detected with Rhodamine-conjugated streptavidin (red) and shows deep penetrance at E11.5, while biotin staining was confined to the epicardial layer at E18.5. The cardiac myosin marker MF20 was used to stain the myocardium (green) and nuclear Hoechst stain (blue). Scale bars, 100 μ m (A) and 20 μ m (B).

Fig. S6

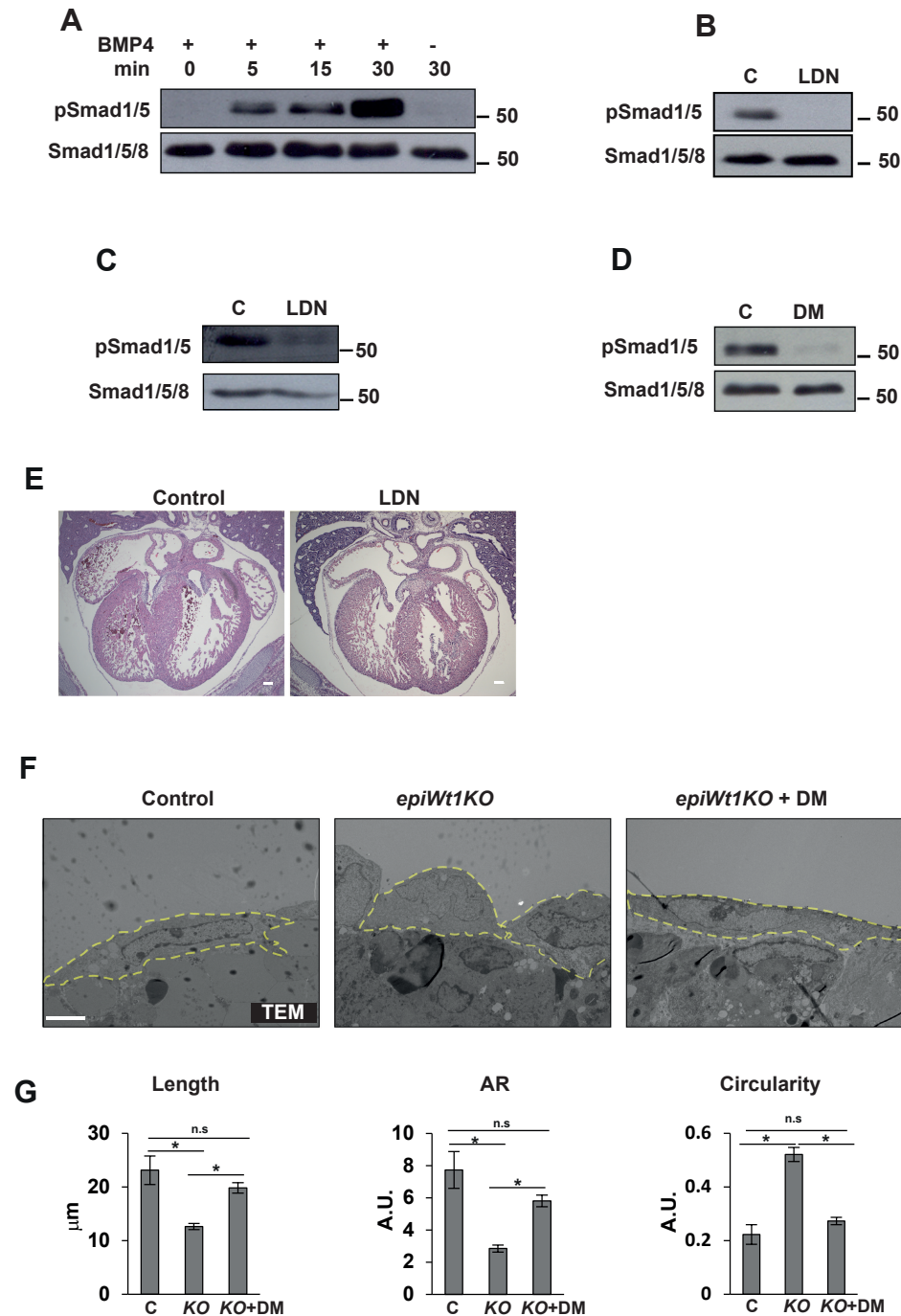


Figure S6. Inhibition of BMP4 signalling rescues the flattening defects in *epiWt1KO* hearts. (A) BMP4 induces the phosphorylation of Smad1 and Smad5 in epicardial cells. Immortalised epicardial cells were pre-treated for 18 hours with dorsomorphin before BMP4 stimulation for indicated time points. Cell lysates were analysed by Western blotting with antibodies against phosphorylated Smad1/5 (P-Smad1/5) and Smad1/5/8 as a loading control. Cell extracts from control (C) and LDN-193189 (LDN)-treated immortalised epicardial cells (B), embryonic heart extracts from control and LDN-193189 (LDN)-treated pregnant mice (C) and cell extracts from DMSO (Control) and dorsomorphin (DM) treated immortalised epicardial cells (D) were analysed by Western blotting with indicated antibodies. (E) H&E staining of E15.5 embryonic heart sections from control and LDN-193189 (LDN)-treated pregnant mice. (F) TEM of control and *epiWt1KO* hearts treated *ex vivo* with DMSO (Control) or dorsomorphin (DM) for 48h. Rescue of the flattening phenotype in epicardial *epiWt1KO* cells in the presence of DM can be observed. (G) Quantification of epicardial cell length, aspect ratio (AR) and circularity are shown as mean \pm s.e.m. Three independent embryos were assessed per condition, and at least 20 epicardial cells were quantitated. Significance was determined by Tukey's multiple-comparison after one-way ANOVA (* $P < 0.05$, n.s. = not significant). Scale bars, 100 μ m (E) and 5 μ m (F).

Table S1. Differentially expressed genes in the *Wt1GFP⁺⁺* epicardial-enriched cell population compared to the *Wt1GFP⁺* population of cells.

[Click here to Download Table S1](#)

Table S2. Cluster analyses of modulated genes in the *Wt1GFP⁺⁺* epicardial-enriched cells.

[Click here to Download Table S2](#)

Table S3. Links to *in situ* hybridisations from the Eurexpress database (www.eurexpress.org) showing the expression of indicated genes in the epicardium.

Gene	Cluster	Link
<i>Upk3b</i>	1	http://www.eurexpress.org/ee/databases/assay.jsp?assayID=euxassay_016996&image=01
<i>Bmp4</i>	1	http://www.eurexpress.org/ee/databases/assay.jsp?assayID=euxassay_017884&image=01
<i>Cdkn1c</i>	1	http://www.eurexpress.org/ee/databases/assay.jsp?assayID=euxassay_018567&image=01
<i>Alcam</i>	1	http://www.eurexpress.org/ee/databases/assay.jsp?assayID=euxassay_003463&image=01
<i>Fbln2</i>	1	http://www.eurexpress.org/ee/databases/assay.jsp?assayID=euxassay_011955&image=01
<i>Capn6</i>	1	http://www.eurexpress.org/ee/databases/assay.jsp?assayID=euxassay_006493&image=01
<i>Gucy1a3</i>	1	http://www.eurexpress.org/ee/databases/assay.jsp?assayID=euxassay_012078&image=01
<i>Pmp22</i>	1	http://www.eurexpress.org/ee/databases/assay.jsp?assayID=euxassay_017431&image=01
<i>Fn1</i>	1	http://www.eurexpress.org/ee/databases/assay.jsp?assayID=euxassay_001464&image=01
<i>Adamts2</i>	2	http://www.eurexpress.org/ee/databases/assay.jsp?assayID=euxassay_003619&image=01
<i>Col1a1</i>	2	http://www.eurexpress.org/ee/databases/assay.jsp?assayID=euxassay_001885&image=01
<i>Col3a1</i>	2	http://www.eurexpress.org/ee/databases/assay.jsp?assayID=euxassay_004670&image=01

Col14a1	2	http://www.eurexpress.org/ee/databases/assay.jsp?assayID=euxassay_001452&image=01
Hba-a1	2	http://www.eurexpress.org/ee/databases/assay.jsp?assayID=euxassay_002328&image=01
S100a1	2	http://www.eurexpress.org/ee/databases/assay.jsp?assayID=euxassay_007368&image=01
Dhrs7	2	http://www.eurexpress.org/ee/databases/assay.jsp?assayID=euxassay_000191&image=01
Eln	2	http://www.eurexpress.org/ee/databases/assay.jsp?assayID=euxassay_004329&image=01
Prnp	2	http://www.eurexpress.org/ee/databases/assay.jsp?assayID=euxassay_007857&image=01
Slit2	3	http://www.eurexpress.org/ee/databases/assay.jsp?assayID=euxassay_017890&image=01
Mfap4	3	http://www.eurexpress.org/ee/databases/assay.jsp?assayID=euxassay_014283&image=01
Reln	3	http://www.eurexpress.org/ee/databases/assay.jsp?assayID=euxassay_017891&image=01
Col1a2	4	http://www.eurexpress.org/ee/databases/assay.jsp?assayID=euxassay_004456&image=01
Igfbp5	4	http://www.eurexpress.org/ee/databases/assay.jsp?assayID=euxassay_001623&image=01
S100a6	4	http://www.eurexpress.org/ee/databases/assay.jsp?assayID=euxassay_017625&image=01
S100a10	4	http://www.eurexpress.org/ee/databases/assay.jsp?assayID=euxassay_018301&image=01
Msln	4	http://www.eurexpress.org/ee/databases/assay.jsp?assayID=euxassay_001942&image=01
Serping1	4	http://www.eurexpress.org/ee/databases/assay.jsp?assayID=euxassay_000667&image=01

Nbl1	4	http://www.eurexpress.org/ee/databases/assay.jsp?assayID=euxassay_000822&image=01
-------------	---	---

Table S4. Differentially expressed genes in *Wt1GFP⁺⁺* epicardial-enriched cells in *epiWT1KO* vs control mice.

[Click here to Download Table S4](#)

Table S5. Differentially expressed genes in *Wt1GFP⁺⁺* epicardial-enriched cells in *epiWT1KO* vs control mice that are modulated during development.

[Click here to Download Table S5](#)

Table S6. List of primers used for genotyping.

Name	Sequence	Annealing
<i>Wt1</i> flox F	TGGGTTCCAACCGTACCAAAGA	58
<i>Wt1</i> flox R	GGGCTTATCTCCTCCCATGT	
Cre F	GCATTACCGGTCGATGCAACGAGTGATGAG	58
Cre R	GAGTGAACGAACCTGGTTCGAAATCAGTGCG	
Cre internal control		
Fabpi200 F	TGGACAGGACTGGACCTCTGCTTTCCTAGA	
Cre internal control		
Fabpi200 R	TAGAGCTTTGCCACATCACAGGTCATTCAG	
<i>Wt1</i> GFP F	GCCTGAAGAACGAGATCAGC	58
<i>Wt1</i> GFP R	GGCAGCTTGAATTCTCTCA	
<i>Wt1</i> GFP F2	AGCCTGAAGCTGCTCACATCC	

Table S7. List of antibodies used in this study.

Name	Company	Reference	Dilution	Technique
Sarcomere myosin (MHC)	DSHB	MF20-s	1:20	IF
WT1	Abcam	ab89901	1:1000	IF
PODXL	R&D	AF1556	1:200	IF
PODOPLANIN	Novus bio	NB600-1015	1:100	IF
Donkey anti-rabbit AF488	Invitrogen	A21206	1:800	IF
Donkey anti-goat AF488	Invitrogen	A11055	1:800	IF
Donkey anti-mouse AF594	Invitrogen	A21203	1:800	IF
Goat anti-hamster AF488	Invitrogen	A21110	1:800	IF
Beta-catenin	BD Transduction	610154	1:250	IF
goat anti-rabbit AF488	Life Technologies	A21200	1:400	IF
goat anti-mouse AF546	Life Technologies	A11003	1:400	IF
p-Smad 1/5	Cell Signaling	41D10	1:1000	WB
Smad1/5/8	Santa Cruz	sc-6031-R	1:1000	WB

Table S8. List of primers used for *in situ* hybridisation probes

Name	Sequence
ISH Tcf21 F	ATGTCCACTGGCTCCCTCAGC
ISH Tcf21 R	CGATGTTAATACGACTCACTATAGGGGAGTTCCACACAAGCGGTTGG
ISH Upk1b F	CCTCTTCTGCTTGTCCGTTCC
ISH Upk1b R	CGATGTTAATACGACTCACTATAGGGCAAATCCAAACCAGGCAACT
ISH Col6a1 F	GAAATGTGACCCAACTGGTCAA
ISH Col6a1 R	CGATGTTAATACGACTCACTATAGGGCAAAGCTAAGCCTCTGGGTGTGT
ISH Col3a1 F	TTGGGATGCAGCCACCTTGG
ISH Col3a1 R	CGATGTTAATACGACTCACTATAGGGGTCCTTTCATACCAGGGA
ISH Reln F	CACACCGTGGACAAAGCAGTA
ISH Reln R	CGATGTTAATACGACTCACTATAGGGGCAGAGAAACCACACATCATTAGC
ISH Emilin1 F	GCTCCCTGAACGACTCACTC
ISH Emilin1 R	CGATGTTAATACGACTCACTATAGGGAAACTCAGGGCAGCTGAAAA
ISH Col1a2 F	ATGAATGGGGCAAGACAATC
ISH Col1a2 R	CGATGTTAATACGACTCACTATAGGGATGTTTCATGGGTTTCTTT
ISH Dcn F	CCTCCTTCTTTCCACACCTG
ISH Dcn R	CGATGTTAATACGACTCACTATAGGGCCATAACGGTGATGCTGTTG

Table S9. List of primers used in ChIP.

Name	Sequence	Annealing
<i>Bmp4</i> prom F	CCCCGCCTCGAAAACCTGG	55
<i>Bmp4</i> prom R	TGTTCTAACCTCGGAAGCGC	
UTR negative control F	AAGACTGGGGAGGAAGGGAA	55
UTR negative control R	AGGGACGGAGACCAGATACT	

Table S10. List of primers used in quantitative real time PCR

Name	Sequence
<i>Wt1</i> F	TTCAAGGACTGCGAGAGAAG
<i>Wt1</i> R	GGGAAAACCTTTCGCTGACAA
<i>Bmp4</i> F	GAGGAGTTTCCATCACGAAGA
<i>Bmp4</i> R	GCTCTGCCGAGGAGATCA
<i>Nppa</i> F	CACAGATCTGATGGATTTCAAGA
<i>Nppa</i> R	CCTCATCTTCTACCGGCATC
<i>Actc1</i> F	CCGATCGTATGCAAAAAGGAA
<i>Actc1</i> R	CTGGAAGGTGGACAGAGAGG
<i>Actn2</i> F	CTCGGAGCTCCATCCAGA
<i>Actn2</i> R	ACTGCTTCAGCTGGTTCATCT
<i>Myh6</i> F	TGCTCAGAGCTCAAGAAGGAT

<i>Myh6</i> R	CCCAGCCATCTCCTCTGTTA
<i>Ttn</i> F	CCGGTGGAAGCTGCTATATT
<i>Ttn</i> R	CCGAGGTTTTACTGCGTA
<i>Upk3b</i> F	CCTGTCCAGATGTGGGATCT
<i>Upk3b</i> R	TCCGAGGATAGTTTGAGAGCA
<i>Dcn</i> F	GAGGGAACTCCACTTGGACA
<i>Dcn</i> R	TTGTTGTTGTGAAGGTAGACGAC
<i>Tcf21</i> F	TGATTAACCTTCTGCCATGAATGA
<i>Tcf21</i> R	AAAAGATACACATTGATAGGCTCTTCT
<i>Dlk1</i> F	GATTCTGCGAGGCTGACAAT
<i>Dlk1</i> R	GGTTCCTTGCAGACTCCATT
<i>Upk1b</i> F	CGATTCCACTGTTTCGTTGC
<i>Upk1b</i> R	GGGCGATGCCACACATAC
<i>Nbl1</i> F	CGCACCCCACTTTCTAGG
<i>Nbl1</i> R	CACCAGGACCCAAAGCAT
<i>Podxl</i> F	TCCTTGTTGCTGCCCTCT
<i>Podxl</i> R	CTCTGTGAGCCGTTGCTG
<i>Smpd3</i> F	GATTGACGGCTGTCATTACCT
<i>Smpd3</i> R	ATGTAATCGCCCTTGAATGC
<i>Krt8</i> F	AGTTCGCCTCCTTCATTGAC
<i>Krt8</i> R	GCTGCAACAGGCTCCACT
<i>Tbx18</i> F	CCGAGACTCTAGGAAC
<i>Tbx18</i> R	TGATGGCCTCGAATGC
<i>Cdkn1c</i> F	TCTCCTTTGCTCGTTT
<i>Cdkn1c</i> R	GGCATTGTGGGTGTTG
<i>18s</i> F	CGATTGGATGGTTTAGTGAGG
<i>18s</i> R	AGTTCGACCGTCTTCTCAGC
<i>Car9</i> F	GCCCAGAAGAAAACAGTGCT
<i>Car9</i> R	CCAAACCTGGGATCTCAATC
<i>Thy1</i> F	GGTGGCAGAAGAAGACAAGG
<i>Thy1</i> R	CCTTCCTGCACGGACTTAGA
<i>Figf</i> F	GCAACTTTCTATGACTGAAACAC
<i>Figf</i> R	TCTCTCTAGGGCTGCATTGG
<i>Slc9a3r1</i> F	CCCTTCAGCAATGGAGAGATAC
<i>Slc9a3r1</i> R	TGGGGCTCTCTGAAGCTG
<i>Krt7</i> F	GGAGATGGCCAACCACAG
<i>Krt7</i> R	GGCCTGGAGTGTCTCAAACCT
<i>Krt14</i> F	ATCGAGGACCTGAAGAGCAA
<i>Krt14</i> R	TCGATCTGCAGGAGGACATT
<i>Krt17</i> F	GGAGCTGGCCTACCTGAAG
<i>Krt17</i> R	ACCTGGCCTCTCAGAGCAT
<i>Coll2a1</i> F	GACAGATGAGACTACGGACAGTTTT
<i>Coll2a1</i> R	TGGTCTGTATCTAATCCGATACCTT
<i>Colla2</i> F	CGGAGAAGCTGGATCTGC
<i>Colla2</i> R	CAGGAGGACCCATTACACCA
<i>Fah</i> F	CCTGCAGACTCTTAGACATGGA

<i>Fah</i> R	GATTGGCTCTCCGAATCTGT
<i>Col1a1</i> F	CATG TTCAGCTTTGTGGACCT
<i>Col1a1</i> R	GCAGCTGACTTCAGGGATGT
<i>Cdkn2b</i> F	AATAACTTCCTACGCATTTTCTGC
<i>Cdkn2b</i> R	CCCTTGGCTTCAAGGTGAG
<i>Cldn15</i> F	GTGGAGACCTTCGGCTTCTT
<i>Cldn15</i> R	AAGGGTCAACCCAGCAT
<i>Egfr</i> F	GCCACGCCAACTGTACCTAT
<i>Egfr</i> R	GCCACACTTCACATCCTTGA
<i>Slit2</i> F	CAGATCTCTGAACTTGCACCA
<i>Slit2</i> R	TGTGATTTTATTTCCATACAGGACA
<i>Ccnd2</i> F	CACCGACA ACTCTGTGAAGC
<i>Ccnd2</i> R	TCCACTTCAGCTTACCCAACA
<i>Cdk4</i> F	AGCGTAAGATCCCCTGCTTC
<i>Cdk4</i> R	ATAGGCACCGACACCAATT
<i>Hes1</i> F	ACACCGGACAAACCAAAGAC
<i>Hes1</i> R	CGCCTCTTCTCCATGATAGG
<i>Nfatc1</i> F	CCACGCCTTCTACCAGGTC
<i>Nfatc1</i> R	GGACTTTGGTGTGGACAGG
<i>Col1a1</i> F	CATG TTCAGCTTTGTGGACCT
<i>Col1a1</i> R	GCAGCTGACTTCAGGGATGT
<i>Igfbp2</i> F	GCCCCCTGGAACATCTCTACT
<i>Igfbp2</i> R	TCCGTTCAGAGACATCTTGCA
<i>Ncam1</i> F	AGGGCAAGGCTGCTTTCT
<i>Ncam1</i> R	CCCCATCATGGTTTGGAGT
<i>Emcn</i> F	GCTCTGGTGGGTTTGTATCGAA
<i>Emcn</i> R	GCTGATCATTCCGTTTTC